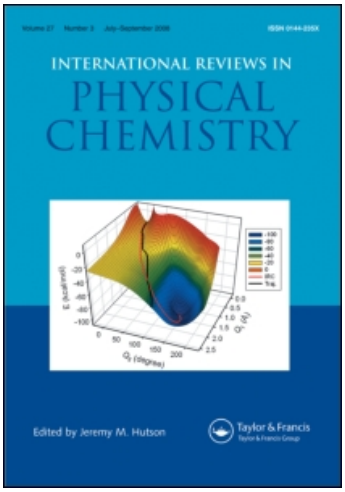

International Reviews in Physical Chemistry
Publication details, including instructions for authors and subscription information:
http://www.informaworld.com/smpp/title~content=t713724383

Molecular rotation in the presence of intramolecular vibrational energy redistribution

John Keske[a]; David A. Mcwhorter[a]; Brooks H. Pate[a]
[a] Department of Chemistry, University of Virginia, Charlottesville, VA, USA

Online publication date: 26 November 2010

To cite this Article Keske, John , Mcwhorter, David A. and Pate, Brooks H.(2000) 'Molecular rotation in the presence of intramolecular vibrational energy redistribution', International Reviews in Physical Chemistry, 19: 3, 363 — 407
To link to this Article: DOI: 10.1080/01442350050034171
URL: http://dx.doi.org/10.1080/01442350050034171

INT. REVIEWS IN PHYSICAL CHEMISTRY, 2000, VOL. 19, NO. 3, 363–407

Molecular rotation in the presence of intramolecular vibrational energy redistribution

JOHN KESKE, DAVID A. McWHORTER†
and BROOKS H. PATE‡
Department of Chemistry, University of Virginia,
Charlottesville, VA 22901, USA

At high energy, the vibrational dynamics of a polyatomic molecule are qualitatively different from the separable normal-mode dynamics that characterize the low energy region of the spectrum. Once the total rovibrational state density exceeds 10–100 states cm^{-1}, the effects of intramolecular vibrational energy redistribution (IVR) are readily observed in the frequency-domain spectrum. In an energy region where IVR occurs, the time scale for the flow of vibrational energy is comparable to the time scale for molecular rotation. The jostling of nuclear positions caused by the IVR dynamics leads to a time-dependent moment of inertia for the molecular rotation. The time-dependent modulation of the moment of inertia, in turn, affects the appearance of the rotational spectrum of the molecule. These effects can be described by the motional narrowing formalism first developed for nuclear magnetic resonance spectroscopy. We present a basic description of the rotational problem for the case where the molecule has a single energetically accessible nuclear geometry and the case where the total energy of the molecule is above the barrier to isomerization. In the latter case, the microcanonical isomerization rate can be obtained from the overall line shape of the rotational spectrum. An example of using rotational spectroscopy to measure the isomerization rate of 4-chlorobut-1-yne at 3330 cm^{-1} is presented.

1. Introduction: models of intramolecular vibrational energy redistribution and conformational isomerization

This review describes our recent work on the rotational spectroscopy of molecules excited to an energy where intramolecular vibrational energy flow occurs. We focus on two aspects of this work: (1) the description of the rotational motion of a highly excited molecule and (2) the measurement of microcanonical rate constants for conformational isomerization reactions. The first topic, which comprises most of this review, provides the theoretical framework for high-resolution spectroscopy of single quantum states of the molecular Hamiltonian in energy regions where intramolecular vibrational energy redistribution (IVR) occurs. Here we present the ways that our understanding of molecular rotational spectroscopy must be amended from the simple theory used for quantum states at low energy (e.g. the pure rotational levels of the molecule) [1, 2]. The development of the theory for this problem uses the motional, or exchange, narrowing theories that were originally developed for nuclear magnetic resonance (NMR) spectroscopy [3, 4].

The second goal of this review is to present an application of this new form

† Current address: Laser Applications Group, National Institute of Standards and Technology, Gaithersburg, MD 20899, USA.
‡ E-mail: bp2k@virginia.edu

International Reviews in Physical Chemistry ISSN 0144-235X print/ ISSN 1366-591X online
http://www.tandf.co.uk/journals

of high-resolution molecular spectroscopy to the field of chemical kinetics. The problem we address is the kinetics of unimolecular isomerization reactions. A unique feature of the measurement technique is that we are able to directly measure the microcanonical rate constant for isomerization, $k(E, J)$. In unimolecular reaction rate theory, this rate constant is often calculated via statistical theories such as the widely used Rice, Ramsperger, Kassel and Marcus (RRKM) theory [5, 6]. By contrast, most other kinetics techniques measure the canonical rate constant, $k(T)$. Additional complexity is added to the unimolecular reaction theory in this case. For example, the efficiency of collisional excitation, a difficult problem in its own right, must be determined in order to calculate the ensemble average rate constant. Therefore, using the measurement methods described in this review it is possible to explicitly test the validity of the fundamental assumptions in statistical theories. To this point in our work, we find that RRKM theory grossly overestimates the microcanonical rate constant for the conformational isomerization process.

Additionally, through a combination of high-resolution infrared spectroscopy and our new methods for rotational spectroscopy of highly excited molecules we can gain some insight into the extent of mode-specificity in fundamental kinetics processes. This ability derives from the fact that infrared absorption spectroscopy and the rotational spectroscopy of 'statistically mixed' quantum states measure qualitatively different types of dynamics. These differences are an example of the principle that guides spectroscopic studies of chemical dynamics: 'what you pluck is what you see' [7]. The infrared spectrum provides mode-specific information about the fundamental chemical processes, such as IVR, following energy deposition in a single vibrational mode. In our infrared studies this initial vibrational mode is a bond-localized hydride stretch motion. Our new rotational measurement techniques work in the opposite limit. We use long-pulsed laser excitation to excite single quantum states of the full molecular Hamiltonian. With respect to a normal-mode vibration basis set, these quantum states are highly mixed. In a time-dependent view of the spectroscopy, we have allowed the molecule to 'statistically relax' during the excitation step. The subsequent rotational spectroscopy that we perform measures the 'ensemble average' dynamics of the molecule. As will be illustrated for the case of isomerization, the mode-specific (infrared) and statistically relaxed (single eigenstate rotational spectroscopy) dynamics can behave quite differently. Therefore, we are uniquely able to quantify the extent of mode-specificity in the isomerization kinetics.

We have omitted any discussion of experimental techniques in this review. Instead we focus on the essential features of the spectroscopy and the way that it can be used to study isomerization kinetics. The reader can find the details of our experimental approach in the recent literature [8, 9, 10]. We expect that new experimental techniques with higher sensitivity will emerge in the future to extend the scope of chemical problems that can be studied through this form of spectroscopy.

1.1. *Frequency domain measurements of intramolecular dynamics*

The theoretical foundation for the rotational spectroscopy of highly excited quantum states is the description of high-resolution spectroscopy in regions where intramolecular energy flow occurs. This description of spectroscopy was first developed in the context of radiationless transitions for excited state processes and is illustrated by the 'standard model' for IVR shown in figure 1 [11, 12, 13]. The description is general and also applies to IVR in the ground electronic state, which is the starting point for this work. In this general formulation, the full molecular

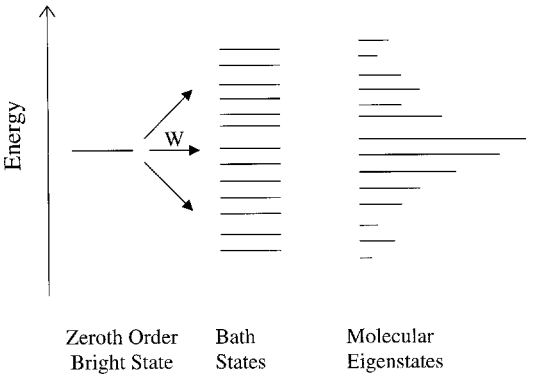

Figure 1. A standard model for IVR. The 'bright' zeroth-order state has some transition probability from the ground state. Nearby in energy there is a set of 'dark' or bath states with zero transition probability from the ground state. The interaction (W) between the bright and bath states (equation (1.2)) produces the set of molecular eigenstates (equation (1.3)). The intensity of each eigenstate in the observed spectrum is proportional to contribution that the bright state makes to the molecular eigenstate composition (equation (1.4)).

Hamiltonian is divided into a simple, zeroth-order term, H_0, and the higher-order interactions in the Hamiltonian, W.

$$H = H_0 + W. \tag{1.1}$$

For the IVR process, H_0 is usually taken to be the molecular Hamiltonian for the normal-mode vibration and distortable-rotor problem [14, 15]. In the most general case, the eigenfunctions are direct products of the vibrational wavefunctions (themselves direct products of the $3N$–6 harmonic oscillator wavefunctions for each normal mode) and an asymmetric-top rotational wavefunction

$$\left|\ {}^{(0)}\right\rangle = |\overline{v}\rangle\,|J_{KaKc}\rangle = |v_1, v_2, \ldots, v_{3N-6}\rangle\,|J_{KaKc}\rangle. \tag{1.2}$$

The remaining terms in the Hamiltonian (W) lead to interactions between the eigenfunctions of H_0 through anharmonic or rotationally mediated (e.g. Coriolis or centrifugal interactions [16]) coupling mechanisms. There are two sets of functions used to describe the spectroscopy and dynamics in IVR. The first set, the eigenfunctions of H_0, are given by equation (1.2). The second set are the eigenfunctions of the full Hamiltonian, H. The quantum states associated with the full Hamiltonian are often called the exact molecular eigenstates (or just the molecular eigenstates). By completeness, the molecular eigenstates can be represented in the zeroth-order basis

$$|\phi_i\rangle = c_b\left|\ {}^{(0)}_{b}\right\rangle + c_1\left|\ {}^{(0)}_{1}\right\rangle + c_2\left|\ {}^{(0)}_{2}\right\rangle + \cdots. \tag{1.3}$$

It is often the case that only a single eigenfunction of H_0 in the energy region of interest has appreciable transition intensity from the ground vibrational state. This eigenstate of H_0 is then called the 'bright' state and is denoted by $\left|\ {}^{(0)}_{b}\right\rangle$ in equation (1.3). The remaining eigenfunctions of H_0 are called the 'dark' states or bath states.

In the ideal high-resolution infrared spectroscopy measurement, the spectrum is fully resolved to the molecular eigenstate level. In this case, the intensity for each transition to a single eigenstate is determined by the character of the bright state in

the eigenfunction

$$I_i = |\langle \phi_i|\mu|\overline{0}, J_{KaKc}\rangle|^2 = |c_b|^2|\langle \overset{(0)}{b}|\mu|\overline{0}, J_{KaKc}\rangle|^2, \tag{1.4}$$

where the initial state is assumed to be a pure rotational level. The sum of the intensities for all eigenstates is conserved and equal to the intensity of the bright-state transition in the zeroth-order basis set. Over the past decade there have been significant advances in molecular beam spectroscopy techniques that make it possible to obtain eigenstate-resolved spectra of large polyatomic molecules [17, 18, 19, 20, 21]. In particular, double-resonance techniques have been developed that provide simplification of the complicated spectra that result from the combination of fragmentation of infrared intensity by IVR dynamics and the overlap of rovibrational transitions [8, 22, 23]. As a result, it is possible to obtain fully state-resolved information about the IVR dynamics.

Eigenstate-resolved spectroscopy of large polyatomic molecules is aimed at measuring the time scale for IVR [21, 24]. From a fully-resolved rovibrational spectrum, the dynamics for the IVR process of the bright state can be calculated. The frequency and relative intensity information in the high-resolution spectrum is sufficient to calculate a single dynamical quantity, the survival probability of the bright state given by [25]

$$P(t) = |\langle \Psi(0)|\Psi(t)\rangle|^2 = |\langle \overset{(0)}{b}|\Psi(t)\rangle|^2 = \sum_i \sum_j I_i I_j \cos\left(\frac{E_i - E_j}{\hbar} t\right). \tag{1.5}$$

This calculation provides the same dynamical information that would be obtained in the ideal single-colour, pump-probe measurement in the time domain [26, 27]. For excitation with a short laser pulse, the initial state ($\Psi(0)$) created through the molecule–field interaction is the bright state. At energies where IVR operates, this state is not an eigenfunction of the full Hamiltonian and will evolve in time.

For a simple exponential decay of the survival probability, the line shape *pro le* of the eigenstate-resolved spectrum is Lorentzian. Because the system is bound for a stable molecule, there are discrete eigenstates of the Hamiltonian. The high-resolution spectrum will consist of a set of transitions whose intensities fluctuate around the smooth line shape profile [28]. The homogeneous line width of a *single eigenstate transition* is determined by the infrared fluorescence lifetime of the state (this lifetime contribution is not included in equation (1.5)). However, the key spectral feature used to interpret mode-specific IVR dynamics is the overall line shape profile. An experimental example of a high-resolution infrared spectroscopy measurement of the IVR dynamics, and the survival probability calculated from the spectrum, is shown in figure 2 [29].

This standard model of IVR and the connection to high-resolution spectroscopy is often criticized based on the fact that the choice of the zeroth-order basis set is arbitrary. However, there are good reasons to choose the normal-mode–distortable rotor basis set for this problem. Most importantly, the transition dipole operator is (nearly) diagonal in this basis set. Therefore, it is easy to determine the nature of the excited state following coherent, short-pulse excitation (i.e. the eigenstate of H_0 that has a non-zero transition dipole matrix element). In this sense, the light field suggests an appropriate basis set for the problem. In a dynamics sense, the zeroth-order basis set we have chosen is a good basis for the short-time dynamics. Secondly, the chosen basis set is convenient for a physical description of the IVR process. The

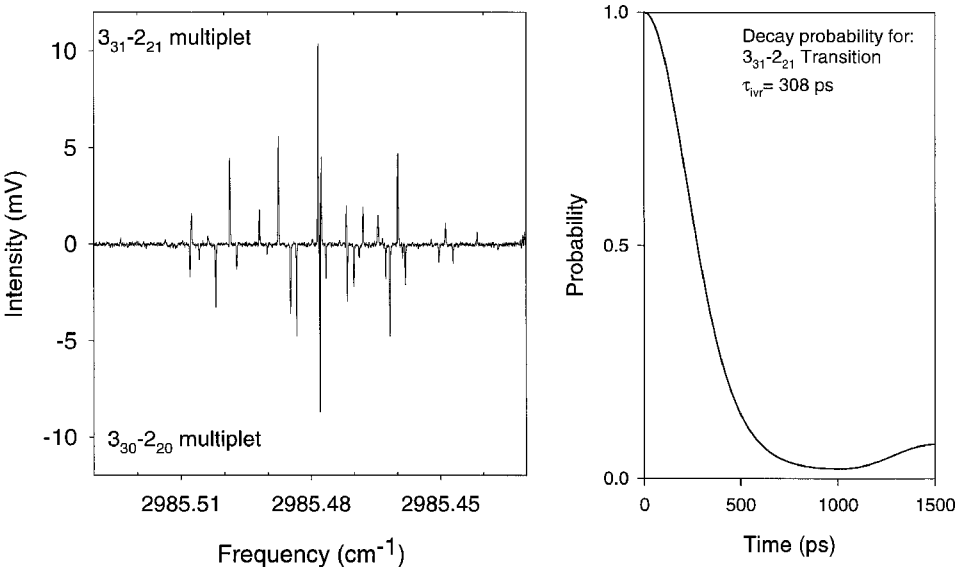

Figure 2. A high-resolution infrared spectra of 2-fluoroethanol. The extensive fragmentation of the spectra is an indication of IVR. This spectra is taken using an electric resonance optothermal spectrometer (EROS) [8]. Using a microwave-infrared technique two spectra (3_{31}–2_{21} (top) and 3_{30}–2_{20} (bottom)) are recorded at the same time, with opposite phase. The survival probability calculated from the 3_{31}–2_{21} spectrum is shown on the right giving an IVR lifetime of 308 ps.

normal-mode nuclear motions can be calculated and visualized in a straightforward manner. Especially simple physical pictures of the initial nuclear motion 'plucked' by the light field occur when the bright state is a local-mode motion, such as an isolated hydride stretch.

A strong limitation to high-resolution spectroscopy (or, equivalently, single-colour pump-probe measurements in the time domain) is that the survival probability constitutes the only dynamical quantity directly available from the spectrum. Direct information about the pathways and time scales of subsequent events in the energy redistribution process is unavailable from the high-resolution measurement. The important chemical questions of where does the energy go and how does it get there remain largely unanswered by this experimental approach. Additionally, the measurement provides quantitative information about the dynamics of a *single* zeroth-order state. This state may be one of thousands to millions (and more) of quantum states in each 1 cm^{-1} interval of a large polyatomic molecule even at low energy (3000 cm^{-1}). The dynamics of the bright states may not be indicative of the average dynamics in the energy region [30, 31, 32]. The techniques described in this review take steps to address these basic limitations by providing ways to determine the average IVR rates in a given energy region and to investigate subsequent dynamical events, such as isomerization, in the IVR process.

1.2. *Spectroscopic model for isomerization kinetics*

In the case where a molecule can undergo isomerization, the simple model for IVR shown in figure 1 needs to be augmented. We are interested in the rotational spectroscopy of a molecule excited to an energy that exceeds the barrier to

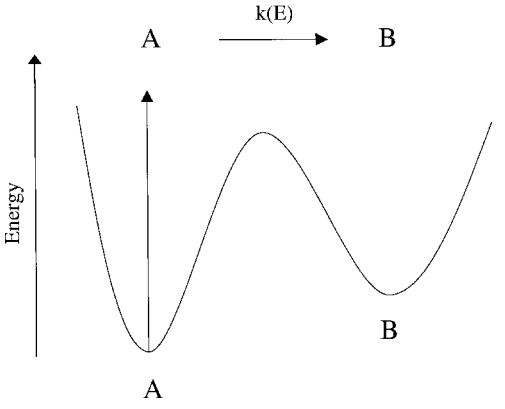

Figure 3. Generalized isomerization reaction potential. If a molecule (A) is excited to an energy above the barrier to isomerization it can isomerize (A → B) at a rate described by the microcanonical rate constant $k(E)$.

isomerization, as depicted in figure 3. Isomerization reactions have a key feature that strongly influences the spectroscopy: the Hamiltonian remains bound during reaction [33]. Therefore, unlike the case of unimolecular dissociation where a true continuum exists, the quantum states involved in the dynamics are discrete molecular eigenstates. To describe the conformational properties of the quantum states above the barrier to isomerization we use the model shown in figure 4 [34]. In this model, we adiabatically separate the torsional coordinate, which is the reaction coordinate for isomerization, from the other normal-mode vibrational coordinates. For each of the normal-mode states we define an effective torsional potential. In most cases it is expected that the torsional potential for the normal-mode vibrational state will have a similar shape to the potential for the ground vibrational state.

In this picture, the different torsional surfaces built upon the normal-mode vibrational states resemble different electronic states. The spectroscopy between torsion–vibrational states would be expected to behave in a similar manner to vibrational spectroscopy between electronic states in the Franck–Condon approximation. Experimentally this model is validated by the fact that the torsional dependence of normal-mode vibrational frequencies is small, except for a few modes that are obviously coupled to the reaction coordinate [35, 36, 37]. Additionally, the infrared spectrum is typically dominated by transitions where the torsional quantum number remains unchanged. In the context of the adiabatic model, this fact suggests that the Franck–Condon-like overlap between torsional states of different normal-mode states is dominated by the diagonal term and, therefore, the shapes of the potential are nearly the same.

The torsion-normal-mode direct product states can be used as the zeroth-order basis set for discussing intramolecular dynamics and isomerization. In this model, there are basis states with energies exceeding the barrier to isomerization that still have well-defined conformational structure. For example, the energy of the hydride stretch normal-mode state is about 3000 cm^{-1} above the ground vibrational state whereas typical barriers to conformational isomerization are about 1000 cm^{-1}. In the model of figure 4, the spectroscopy of the hydride stretch would involve a transition from the lowest torsional state of the ground vibrational state to the

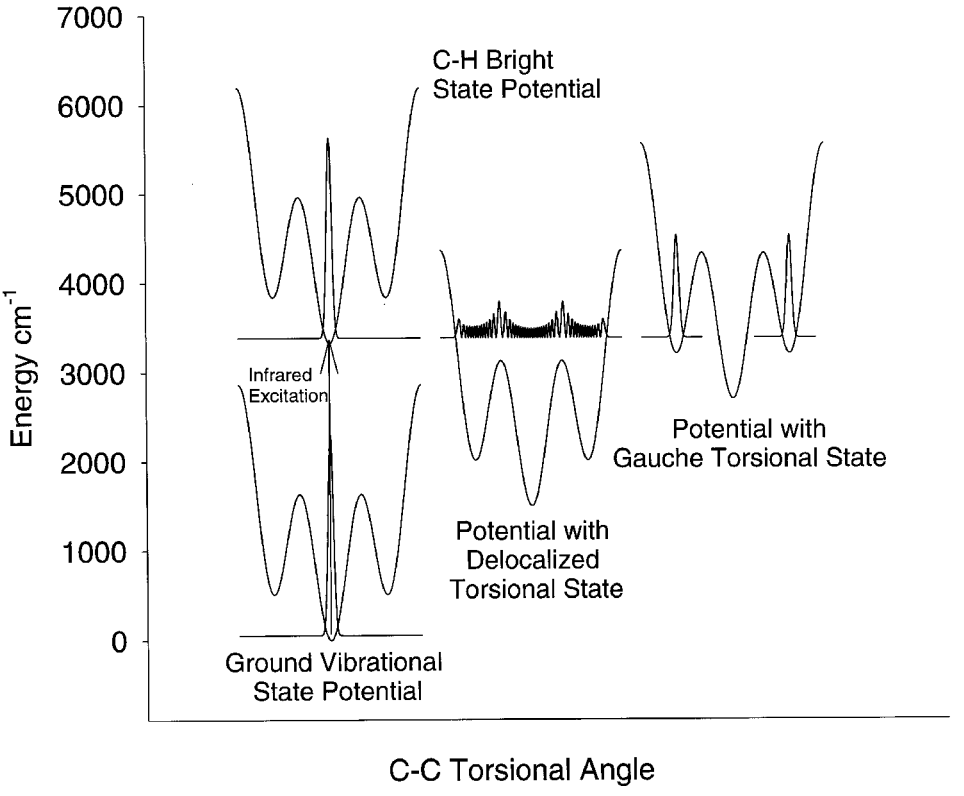

Figure 4. One-dimensional torsional isomerization problem. With this zeroth-order description isomerization occurs due to interactions between states localized around different minima. Each normal-mode vibrational state has its own potential energy curve. For clarity, the torsional potentials for the two 'bath' states have been shifted. In this energy region, the zeroth-order C–H stretch bright state can couple to delocalized torsional states or states from a different conformer that have approximately the same energy. These interactions produce 'structurally mixed' eigenstates of the full Hamiltonian.

lowest torsional state in the potential built on the hydride stretch. Both initial and final states have well-defined conformational structure. This model just reflects the fact that vibrational excitation of the hydride stretch is expected to simply 'pluck' the C–H stretch, leaving the conformational structure unchanged. As will be shown later, the rotational band contours of the hydride stretches usually have structures characteristic of the lowest energy conformer. In other words, the bright state does have a well-defined conformational geometry as suggested by the model.

Using the torsion–normal-mode basis set we can now consider the effects caused by intramolecular vibrational energy redistribution. The intramolecular interactions in the Hamiltonian will mix the zeroth-order basis states that have approximately the same total energy. In this model, the near-resonant basis states include quantum states with geometries localized around the different stable minima of the torsional surface as well as states where the torsional wavefunction is delocalized over the full torsional space. The interaction terms in the Hamiltonian will lead to molecular eigenstates that contain contributions from all of the interacting basis states. In

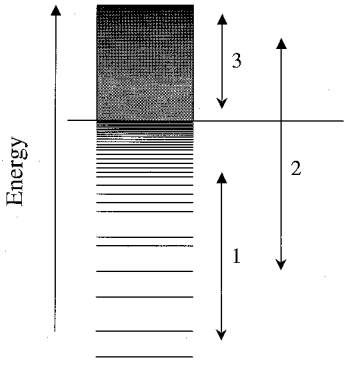

Figure 5. A simplified diagram of the rovibrational quantum states of a polyatomic molecule. At low energy the states are separable and the normal-mode approximation is valid. Above a threshold energy, the state density is sufficiently high (> 10 states cm^{-1}) that the quantum states are mixed through IVR. Spectroscopy between these states can be divided into three types. (1) Spectroscopy between the low energy states, which follows the usual rotation–vibration description [1, 2]; (2) spectroscopy from a low energy state into the highly mixed regime (IVR measurements, see figure 1); (3) spectroscopy between the highly mixed states (the subject of this review).

this sense, the wavefunctions contain contributions from reactant, product and the delocalized states. We have called the quantum states in this regime 'structurally mixed' [34].

1.3. *Types of spectroscopy for polyatomic molecules*

The previous sections provided a description of high-resolution rotation–vibration spectroscopy for molecules where IVR occurs and the relationship of the spectrum to mode-specific intramolecular dynamics. From an extensive set of experiments it has been found that the characteristics of spectroscopy in this regime, e.g. fragmentation of the oscillator strength over several molecular eigenstates, become prevalent when the rovibrational state density reaches 10–100 states cm^{-1}[21, 38, 39]. This threshold state density is already reached for the hydride stretch vibrations (3000 cm^{-1}) for medium sized molecules with about 10 atoms [17]. The existence of a well-defined onset for IVR provides a way to characterize the types of spectroscopy that can occur. This description is illustrated in figure 5.

Below the threshold for extensive state-mixing caused by IVR, the quantum states of the Hamiltonian are well approximated by the zeroth-order basis states. Spectroscopy between quantum states below the IVR threshold falls into the category of 'standard' molecular spectroscopy. The energy level patterns and selection rules in this energy regime are well known and are presented in several textbooks on molecular spectroscopy [1, 2, 14, 15]. Of course even in this regime there are problems of great current interest, most notably the spectroscopy of large-amplitude motions in molecules and clusters of molecules [40, 41, 42]. However, for a typical molecule with well-defined nuclear geometry this type of spectroscopy has been described in extensive detail.

The second type of spectroscopy that can be performed involves transitions from a quantum state below the IVR threshold (typically a rotational level of the ground vibrational state) to quantum states above this threshold [21, 24]. The standard theoretical model for this problem is shown in figure 1 and was discussed

in the previous section. In this form of spectroscopy, the final states are *highly mixed* in the zeroth-order basis set that describes the low energy states as indicated in equation (1.3). This state-mixing leads to the observation of several molecular eigenstate transitions where one would expect a single-rovibrational transition based on the selection rules of spectroscopy at low energy. This fragmentation of the oscillator strength is the spectral manifestation of energy flow between the zeroth-order normal-mode vibrational states (see figure 2).

The third type of spectroscopy involves transitions between two quantum states above the IVR threshold. In this case, both states in the transition are highly mixed with respect to the usual spectroscopic basis set. This third type of molecular spectroscopy has received much less theoretical and experimental attention. The problem in this area that has attracted the most interest involves the nature of vibrational spectroscopy [43, 44, 45, 46, 47, 48]. This work has been performed in the context of infrared multiphoton excitation (IRMPE). In the IRMPE literature, the region of highly mixed quantum states is often called the quasi-continuum. The importance of spectroscopy between highly mixed states for understanding the IRMPE process has motivated a few experiments designed to investigate this third type of spectroscopy [49, 50, 51, 52, 53, 54, 55, 56, 57]. These experiments are difficult owing to the inability to cleanly prepare states above the IVR threshold.

With the descriptions of the zeroth-order Hamiltonians for molecules with a single and multiple stable geometric minima, we next proceed to discuss the spectroscopy of *single quantum states* in an energy region where there is extensive state-mixing. Experimentally, we can access these highly mixed quantum states through the hydride stretch fundamentals of medium-large polyatomic molecules. In this sense, the quantum states would not be considered 'highly-excited' and these two concepts need to be kept separate. For example, the spectrum of a highly excited small molecule can still show regular spectroscopic structure with no evidence of state-mixing. Despite the high total energy of the molecule, the spectroscopy would not display the effects we will discuss for highly mixed states [58, 59]. In particular, we focus on rotational motion of the molecule in this regime. New features of the spectroscopy arise from the presence of highly mixed wavefunctions that are described by motional narrowing theory [60, 61, 62]. In the next section we provide a basic description of the rotational motion of a molecule with a single, energetically accessible structure. In the third section of this review, we extend this theory to include the possibility that isomerization occurs.

2. Rotational spectroscopy and IVR dynamics

This section discusses the basic issues involved in the rotational motion of molecules in energy regions where IVR occurs [60, 61]. The discussion is limited to the case where the molecule has a single, energetically accessible conformation. Also, the problem focuses on the rotational spectrum that is measured from a *single* molecular eigenstate. There are two different ways that the IVR dynamics modify the rotational spectrum of the molecule. First, the presence of state-mixing leads to the appearance of statistical properties in the spectrum of a single molecular eigenstate. This change in the spectrum is entirely described through the number of states participating in the IVR dynamics and is, therefore, related to the *extent* of IVR. A second change in the spectrum caused by IVR is observed in the overall line shape of the rotational spectrum. This effect is described by the motional narrowing theories originally developed for NMR spectroscopy [63, 64, 65, 66] and

depends on the *rate* of IVR. Through changes in the line shape of the rotational spectrum, new information about the rate and mechanism of IVR can be obtained that complements that of single-photon infrared studies.

2.1. *Statistical properties of the molecular eigenstates*

The description of the rotational spectrum is based on the choice of a zeroth-order basis. The basis we choose is the 'spectroscopic basis'. In this basis set the quantum states are direct products of normal-mode vibrational states and distortable rotor rotational states (equation (1.2)). Of particular importance for this problem, each normal-mode vibrational state has its own set of rotational constants (e.g. A, B, C and distortion constants). It is common to describe the vibrational dependence of the rotational constants using a series approximation [14, 15]. To lowest order, the rotational constant (B) of a vibrational state can be written as

$$B_{\bar{v}} = B_e - \sum_{i=1}^{3N-6} \alpha_i \left(v_i + \frac{1}{2} \right) = B_0 - \sum_{i=1}^{3N-6} \alpha_i v_i, \tag{2.1}$$

where B_0 is the rotational constant for the ground vibrational state and the constants α_i are called the vibration–rotation interaction constants. Similar expressions can be written for the other rotational and distortion constants. Also, for highly excited molecules it is likely that higher order terms in the expansion would be required, however, there is little or no data in the literature that can assess the importance of these terms.

The vibration–rotation interaction constants contain contributions from two different effects [14, 15]. From a physical point of view, the most important contribution comes from the change in the moment of inertia averaged over the vibrational wavefunction. This vibrational contribution includes both a harmonic contribution (due to changes in the root-mean-squared bond distances and angles) and an anharmonic contribution (where the average bond length and angles are functions of the vibrational states). This contribution, therefore, reflects the physical changes in geometry that accompany vibrational excitation. The second contribution to the vibration–rotation interaction constant comes from non-resonant rovibrational interaction via Coriolis coupling. Because the non-resonant interactions will persist at high energy, they are included in the zeroth-order problem. The problem that we are dealing with is how the extensive local, resonant perturbations in the spectrum that characterize IVR (see figure 2) affect the rotational spectrum of a single molecular eigenstate.

With this definition of the vibration–rotation interaction constants, we can now consider the properties of single molecular eigenstates of a molecule. As indicated in figure 5, there are two energy regimes for the rotational spectroscopy of single quantum states. At low energy, the spectroscopic basis set provides an excellent description of the quantum states. In this regime, the rotational spectroscopy of a single rotation–vibration eigenstate follows the usual description [1, 2]. Here, a single rotational transition is observed in the frequency region characteristic of the rotational motion. This frequency domain spectrum reflects the fact that the rotational motion of the molecule is completely regular and contains a single frequency component. The frequency is determined by the moment of inertia of the molecule averaged over the vibrational wavefunction. Because the vibrational motion is much faster than the rotational period, the rotation can be characterized by a single, vibrationally averaged structure. Note that in this energy regime the

rotational motion is regular even if the wavefunction is widely spread, as might occur for molecules with a large amplitude coordinate [67, 68].

More interesting is the second energy regime of figure 5 where IVR occurs. In this case, the time scale for vibrational energy flow is comparable to the rotational periods so that the molecule can sample different nuclear configurations during the rotational motion. These effects are described by considering the spectroscopic properties of the interacting zeroth-order rovibrational states. In this energy regime, there will be several basis states interacting through anharmonicity (and Coriolis coupling) in the molecular Hamiltonian. Due to the vibration–rotation interaction terms, equation (2.1), each vibrational state has its own set of rotational constants. For some smaller polyatomic molecules the vibration–rotation interaction terms are known for all, or most, of the normal-mode vibrational states. From this information, and assuming the lowest order expansion represented by equation (2.1), the distribution of rotational constants for a local microcanonical ensemble can be calculated. For the cases reported in the literature, the distribution can be approximated by the normal distribution [19, 69, 70]. Therefore, the *ensemble* rotational constant properties of the zeroth-order states can be characterized by the average rotational constant (B_{avg}) and the standard deviation ($\sigma(B)$).

To understand the features of the rotational spectrum of a single quantum state in the IVR regime we must examine the properties not of the zeroth-order ensemble but of the individual molecular eigenstates. To illustrate the eigenstate rotational properties, we employ random matrix model calculations [61]. The properties of the random matrix Hamiltonian have been shown to provide a good description of real spectra in the IVR regime [71, 72]. The model calculations presented below assume that the distribution of rotational constants in the spectroscopic basis set is described by the normal distribution. The statistical rotational properties of the molecular eigenstates can be quantified in terms of the expectation value and uncertainty of the rotational constant in each quantum state using the usual relations

$$\langle B\rangle_i = \sum_j |c_j^{(i)}|^2 B_j^{(0)}, \tag{2.2}$$

$$\begin{aligned}\Delta B_i &= (\langle B^2\rangle_i - \langle B\rangle_i^2)^{1/2} \\ &= \left(\sum_j |c_j^{(i)}|^2 B_j^{(0)2} - \left(\sum_j |c_j^{(i)}|^2 B_j^{(0)}\right)^2\right)^{1/2}.\end{aligned} \tag{2.3}$$

In these expressions, the sums run over the j-zeroth-order contributions to the molecular eigenstate (equation (1.3)) where each zeroth-order state has its own rotational constant ($B_j^{(0)}$) given by equation (2.1).

We consider the statistical distribution of these two quantities in the *molecular eigenstate ensemble*. The evolution of the eigenstate properties as the coupling between the basis states is increased is shown in figures 6 and 7. In these figures, the extent of state-mixing is characterized by the quantities ρW, where ρ is the state density and W is the root-mean-squared interaction matrix element in the Hamiltonian model, and the number of effective states involved in the state mixing. The number of effective states mixed by the IVR dynamics is given by

$$N_{\mathrm{eff}} = \frac{1}{\sum_i |c_b^{(i)}|^4}, \tag{2.4}$$

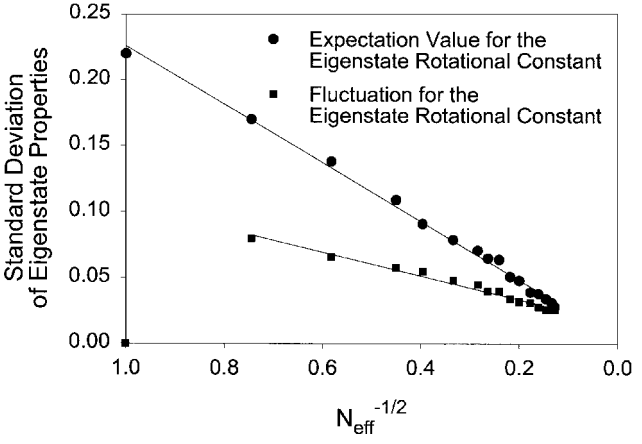

Figure 6. Within the set of molecular eigenstates, there will be a distribution of the rotational constant expectation value (equation (2.2)) and fluctuation (2.3). The standard deviations of these two eigenstate properties are shown as the extent of state-mixing is increased, as measured by the number of effectively coupled states (equation (2.4)). The distribution for both of these quantities narrows linearly with $N_{\text{eff}}^{-1/2}$. This result indicates that for extensive mixing, the statistical properties of all eigenstates are the same.

where the sum runs over all molecular eigenstates and a single zeroth-order state is chosen as the bright state.

These model calculations show how the statistical properties of the original zeroth-order ensemble become imbedded in the character of each molecular eigenstate. In the absence of IVR, where $\rho W = 0$ or $N_{\text{eff}} = 1$, each eigenstate (i.e. each zeroth-order state) has its own rotational constant. In this case, there is no uncertainty in the rotational constant (equation (2.3)), however, there is a spread of expectation values in the ensemble given by the standard deviation of the rotational constant distribution, $\sigma(B)$. This initial condition can be gleaned from figures 6 and 7. Figure 8 shows the average value of the rotational constant uncertainty in the eigenstate ensemble and initially it is zero. The distribution of average rotational constants (equation (2.2)) is shown in figure 6 and is initially the standard deviation of the original zeroth-order ensemble ($\sigma(B) = 0.2$ in the calculation).

As the interaction strength is increased, there are two changes in these quantities. One change is that each eigenstate acquires a fluctuation. This evolution is given in figure 8 where it is found that this quantity very rapidly approaches the original zeroth-order ensemble standard deviation ($\sigma(B)$). The full zeroth-order ensemble limit is reached by the time $\rho W = 1$ [73, 74]. This relative interaction strength corresponds to about 10 states participating in the state-mixing, as indicated by the value of N_{eff}. At the same time, the spread of average rotational constants in the eigenstates, determined by the standard deviation of the eigenstate averages ($\sigma(\langle B \rangle_i)$), gets smaller (figure 6). The narrowing of this distribution is simply given by

$$\sigma\left(\langle B \rangle_i\right) = \frac{\sigma(B)}{N_{\text{eff}}^{1/2}}. \tag{2.5}$$

As shown in figure 6, the spread of values for the rotational constant fluctuation in

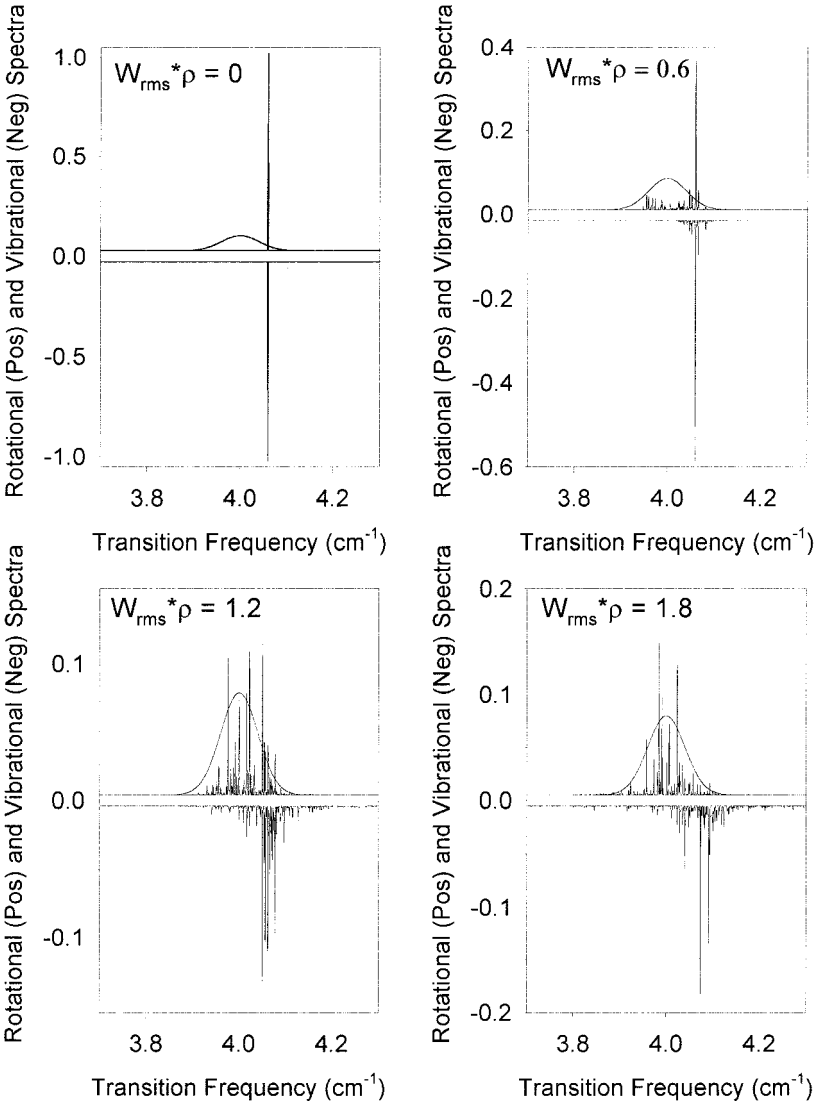

Figure 7. A random matrix model calculation of the evolution of the bright-state vibrational spectrum (negative spectrum) and the single eigenstate rotational spectrum (positive spectrum) is shown as the coupling strength increases (the value of ρW is given in each panel). The vibrational spectrum is for the bright state with total angular momentum $J + 1$. The $\Delta J = +1$ rotational spectrum is calculated for the most intense vibrational transition at total angular momentum J (and, therefore, terminates on eigenstates with $J + 1$ like the vibrational spectra). For no coupling (upper left), the vibrational and rotational spectra both consist of a single transition. As the coupling is increased, the rotational spectrum shifts in frequency and broadens through fragmentation of the spectrum. In the 'fully mixed' limit ($\rho W \sim 1$), the single eigenstate rotational spectrum simply reflects the initial distribution of rotational frequencies in the zeroth-order basis. This distribution is shown by the solid Gaussian line shape profile.

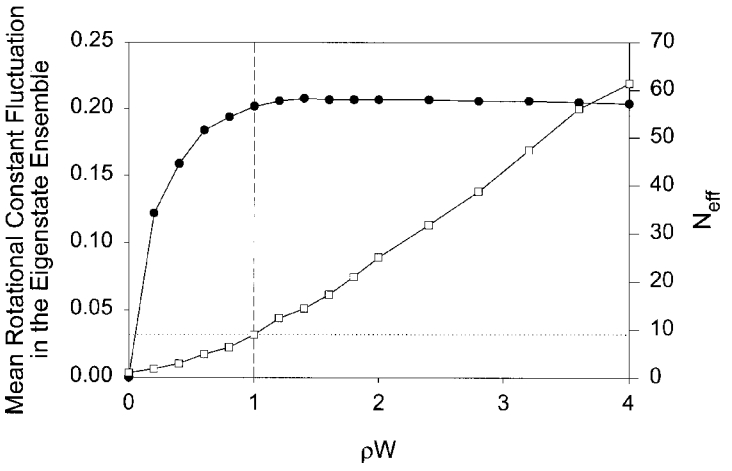

Figure 8. The evolution of the eigenstate-average rotational constant fluctuation (equation (2.3)) is shown as a function of the extent of state-mixing. The extent of state-mixing can be judged from the number of effectively coupled states (equation (2.4)) shown by the open squares on the right hand axis. A rapid convergence of the eigenstate rotational constant fluctuation to the standard deviation of rotational constants in the zeroth-order basis ($\sigma(B) = 0.2$) is observed. The 'fully mixed' limit is reached when $\rho W \sim 1$.

the molecular eigenstates also decreases as $(N_{\text{eff}})^{-1/2}$. These model results indicate that in the presence of extensive state-mixing, the rotational constant average and fluctuations approach the same value for all eigenstates. Furthermore, the quantum mechanical average and fluctuation in a single eigenstate assume the original ensemble average and standard deviation of the zeroth-order ensemble, respectively. In this way, the properties of the microcanonical ensemble are impressed onto the properties of each molecular eigenstate.

2.2. *Calculation of the rotational spectrum of a single quantum state*

The calculation of the spectrum of a single quantum state requires consideration of two features of the spectroscopy: (1) the energy level structure at sequential values of the total angular momentum (J), and (2) the vibrational dependence of the transition moment (which includes the dipole moment and the rotational Hönl–London factors [14, 15]). In this problem, we consider the $\Delta J = +1$ rotational transition for a single quantum state with a well-defined initial total angular momentum (J). To simplify the discussion, it is assumed that the rotational spectrum of interest behaves like the pure rotational spectrum of a linear molecule. For example, this approximation is valid for a near prolate asymmetric top where the effective rotational constant (B_{eff}) for the a-type spectrum is $\frac{1}{2}(B + C)$.

To describe the spectroscopy of a single, highly mixed quantum state it is convenient to work in the basis set where the initial state is an eigenfunction. In this case, the basis set of choice is the set of molecular eigenstates of the full Hamiltonian with total angular momentum quantum number, J. This approach is general for describing the appearance of a spectrum in regions where dynamics occur. For example, for the standard model of IVR shown in figure 1, the problem is described in terms of the basis set where the initial state (e.g. the ground vibrational

state) is an eigenstate (i.e. the eigenstates of H_0). For the rotational spectroscopy of a single, highly mixed state we have called the basis set the 'eigenstate-at-J' basis. The exact nature of the zeroth-order state-mixing in this basis set is determined by the relative energies of the zeroth-order states and the interaction matrix elements between them. One important feature of this problem is that the relative energies of the zeroth-order states at the next higher value of the total angular momentum $(J + 1)$ differ from the ordering at J. The variation in the ordering is caused by the vibrational dependence of the rotational constants. At the higher value of the total angular momentum, the energy of the ith zeroth-order basis state is given by

$$E_i^{(0)}(J + 1) = E_i^{(0)}(J) + 2B_i(J + 1) = E_i^{(0)}(J) + 2B_{\text{avg}}(J + 1) + 2\Delta B_i(J + 1), \quad (2.6)$$

where $E_i^{(0)}(J)$ is its energy at the lower value of angular momentum, B_{avg} is the local zeroth-order ensemble average rotational constant (and will, in general, differ from the rotational constant in the ground vibrational state) and ΔB_i is the deviation of the rotational constant of the ith zeroth-order state from the local ensemble average.

Using this notation, the molecular Hamiltonian at $(J + 1)$ can be written with respect to the zeroth-order basis in the form

$$H(J + 1) = H(J) + 2B_{\text{avg}}(J + 1)\mathbf{I} + 2\Delta B_i(J + 1), \quad (2.7)$$

where each term is a matrix. In this expression, $\mathbf{I}$ is the identity matrix and ΔB_i is a diagonal matrix. The first term, $H(J)$ includes the interaction matrix elements between the zeroth-order basis states: $H(J) = H_0(J) + W$. Also, we assume that the interactions (W) are independent of the total angular momentum (i.e. they represent purely anharmonic interactions). To convert to the 'eigenstate-at-J' basis, a similar transformation is applied that diagonalizes the $H(J)$ part of the full Hamiltonian in equation (2.7). This transformation leads to a new Hamiltonian problem that is formally similar to the basic IVR model of equation (1.1),

$$H(J + 1)_{\text{eigenstate}} = \left[H(J)_{\text{eigenstate}} + 2B_{\text{avg}}(J + 1)\mathbf{I}\right] + 2(J + 1)[\mathbf{C}^{\text{T}}\Delta B_i\mathbf{C}], \quad (2.8)$$

where $H(J)_{\text{eigenstate}}$ is given by $\mathbf{C}^{\text{T}}H(J)\mathbf{C}$ and is diagonal ($\mathbf{C}$ is the eigenvector matrix for the molecular eigenstates with respect to the zeroth-order basis set). The first term in equation (2.8) simply shifts the energies of the eigenstates by the ensemble average rotational frequency. However, in transforming the second term, new off-diagonal interactions are introduced. Therefore, it is found that our chosen quantum state at total angular momentum J is no longer an eigenstate at $(J + 1)$. Therefore, the rotational spectrum of the single eigenstate is expected to show the same fragmentation effects that are found in the standard IVR problem. However, in this case the interaction terms that cause fragmentation of the spectrum originate in the vibration–rotation interaction constants (through the off-diagonal elements of $[\mathbf{C}^{\text{T}}\Delta B_i\mathbf{C}]$).

To complete the description of the spectroscopy, it is also necessary to evaluate the transition moment in the 'eigenstate-at-J' basis. In the original zeroth-order basis, the transition moment will also have a vibrational dependence. The transformation to the 'eigenstate-at-J' basis can be handled in the same way as for the vibrational dependence of the rotational constants. In the 'eigenstate-at-J' basis the transition moment operator is

$$\mu_{\text{eigenstate}} = \mu_{\text{avg}}I + \mathbf{C}^{\text{T}}\Delta\mu_i\mathbf{C}, \quad (2.9)$$

where the same similarity transformation is used that diagonalizes the full Hamil-

tonian at total angular momentum J. The result of this conversion is that there is a dominant 'diagonal' transition moment term in the eigenstate basis given by

$$\langle \phi_i | \mu | \phi_i \rangle = \mu_{\text{avg}} + [\mathbf{C}^{\text{T}} \Delta\mu_i \mathbf{C}]_{ii}. \tag{2.10}$$

This term can be identified as the 'dipole moment' of the ith eigenstate since the vibrational wavefunctions in the matrix element are identical. However, when considering the spectrum from a single initial eigenstate, there are now off-diagonal matrix elements given by

$$\langle \phi_j | \mu | \phi_i \rangle = [\mathbf{C}^{\text{T}} \Delta\mu_i \mathbf{C}]_{ij}. \tag{2.11}$$

In this term, the eigenstate vibrational wavefunction is different in the initial and final states and this term can, therefore, be equated with a 'vibrational' transition dipole moment at the eigenstate level. In the limit of strong state-mixing these 'vibrational' contributions to the spectrum are expected to be small due to dilution of the $\Delta\mu$ term over a large number of eigenstates. Simulations of the changes in the rotational spectrum when a distribution of zeroth-order dipole moments is included supports this conclusion (see figure 8 of [61]).

The general conclusion of this description of the spectroscopy is that we can define a 'pure rotational' spectrum for a single eigenstate that has a transition moment given by equation (2.10). However, the important feature of the spectrum is that the stationary vibrational motions at total angular momentum J (i.e. the vibrational motion associated with a single eigenstate) are no longer stationary at the next value of the total angular momentum $(J + 1)$. At this higher angular momentum level, there will be vibrational energy redistribution driven entirely by the vibration–rotation interaction terms leading to 'rotationally induced IVR'. As a result, the rotational spectrum of the jth single eigenstate will consist of a series of transitions centred at the rotational frequency given by

$$\nu_{\text{centre}}^{(j)} = 2(J + 1)(B_{\text{avg}} + [\mathbf{C}^{\text{T}} \Delta B_i \mathbf{C}]_{jj}). \tag{2.12}$$

Again, in the limit of extensive state-mixing we expect that this centre frequency will be the same for all eigenstates as indicated by figure 6. Physically, at a given energy we expect the average geometry of the molecule to be slightly modified from the geometry in the ground vibrational state. The centre frequency of the rotational spectrum and the 'pure rotational' transition moment reflect this new average geometry of the molecule.

The important problem remains to characterize the line shape of the rotational spectrum of a single quantum state. For these spectra, the line shape is defined as the overall intensity profile of the spectrum. The eigenstate-resolved spectrum will consist of a set of transitions underneath this line shape profile in a manner analogous to the appearance of the high-resolution infrared spectrum in the presence of IVR (figures 1 and 2). The key feature of the spectroscopy is that this line shape profile is a function of the IVR rate between the zeroth-order vibrational states. In terms of the discussion presented above, this can be attributed to the fact that the transformation matrix, $\mathbf{C}$, is a function of the strength of the root-mean-squared vibrational interaction matrix elements. Therefore, the structure of the vibration–rotation 'perturbation' matrix, $[\mathbf{C}^{\text{T}} \Delta B_i \mathbf{C}]$, for the eigenstate rotational problem is also modified by the IVR process.

A model calculation of the rotational spectrum of a single eigenstate as a function of the interaction matrix element is shown in figure 7 [61]. In the absence

of these interactions, the rotational spectrum is simply the 'pure rotational' spectrum of a single vibrationally excited state. It consists of a single transition at the frequency determined by the rotational constant of the zeroth-order state. This type of spectrum would be observed in an infrared-microwave double-resonance spectroscopy measurement at low energy where the vibrational state is unperturbed. Also shown in this figure is the vibrational spectrum calculated for this energy region. In this model calculation, we determine the rotational spectrum of the strongest transition in the rovibrational spectrum. In this simple case of no mixing, the chosen state is simply the zeroth-order bright state. In the rovibrational spectrum of the unperturbed bright state we would observe a single transition to the $(J + 1)$-level of the excited state. Furthermore, the quantum state we observe in the rotational spectrum ($J \rightarrow J + 1$) would be the same one found in the rovibrational spectrum.

As the *extent* of IVR increases, measured by the effective number of coupled states, the spectrum undergoes substantial modification. The rotational spectrum of a single eigenstate evolves in two ways. First of all, the centre position of the spectrum shifts towards the frequency given by the eigenstate average rotational constant (equation (2.12)). Also, there is a broadening of the spectrum. The overall line shape profile becomes Gaussian in the model calculation. This line shape is completely determined by the distribution of rotational constants in the zeroth-order basis set. By the time 'full mixing' is encountered ($\rho W \sim 1$ as indicated in figure 8), the line shape profile of the single quantum state spectrum simply reflects the original zeroth-order rotational constant distribution. The centre position and width of the spectrum are determined by the average value and fluctuation of the rotational constant in the eigenstate (equations (2.2) and (2.3)). Also, the line shape of the rotational spectrum of the single quantum state is qualitatively different from the line shape of the vibrational spectrum. This behaviour simply reflects the fact that the two forms of spectroscopy are sensitive to two different types of dynamics: decay of the vibrational survival probability due to IVR and the rotational motion of the molecule.

Upon further increase of the IVR rate, there is a second characteristic change in the line shape profile. This evolution is shown in figure 9, which is a continuation of the calculation in figure 7. With increasing IVR rate, the width of the spectrum narrows and line shape approaches a Lorentzian form (near line centre). This effect is the well-known motional or exchange narrowing phenomenon first encountered in NMR spectroscopy [63, 64, 65, 66]. In this case, IVR is the cause for this narrowing and we have called this effect 'IVR exchange narrowing'. In the limit of strong narrowing [63, 64, 65, 66], the line width of the spectrum is given approximately by

$$\Delta\nu_{\text{obs}} = \Gamma_{\text{rot}} \frac{\Gamma_{\text{rot}}}{\Gamma_{\text{IVR}}} = 2(J + 1)\sigma(B) \frac{2(J + 1)\sigma(B)}{2\pi \langle W^2 \rangle \rho}, \tag{2.13}$$

where Γ_{rot} is the dephasing rate caused by the spread in zeroth-order rotational frequencies and Γ_{IVR} is the IVR rate in the model calculation (given by the Fermi Golden Rule expression). The Lorentzian line shape with this width is shown in figure 9 along with the original Gaussian distribution of rotational frequencies from the zeroth-order states.

The physical origin of this narrowing effect is described by the following argument. The vibrational interaction matrix elements that lead to IVR can be interpreted as the rate of exchange between the zeroth-order states. When this rate of exchange is slow, we can imagine that the molecule samples each normal-mode rotational frequency on a time scale slow compared to the rotation. This sampling leads to

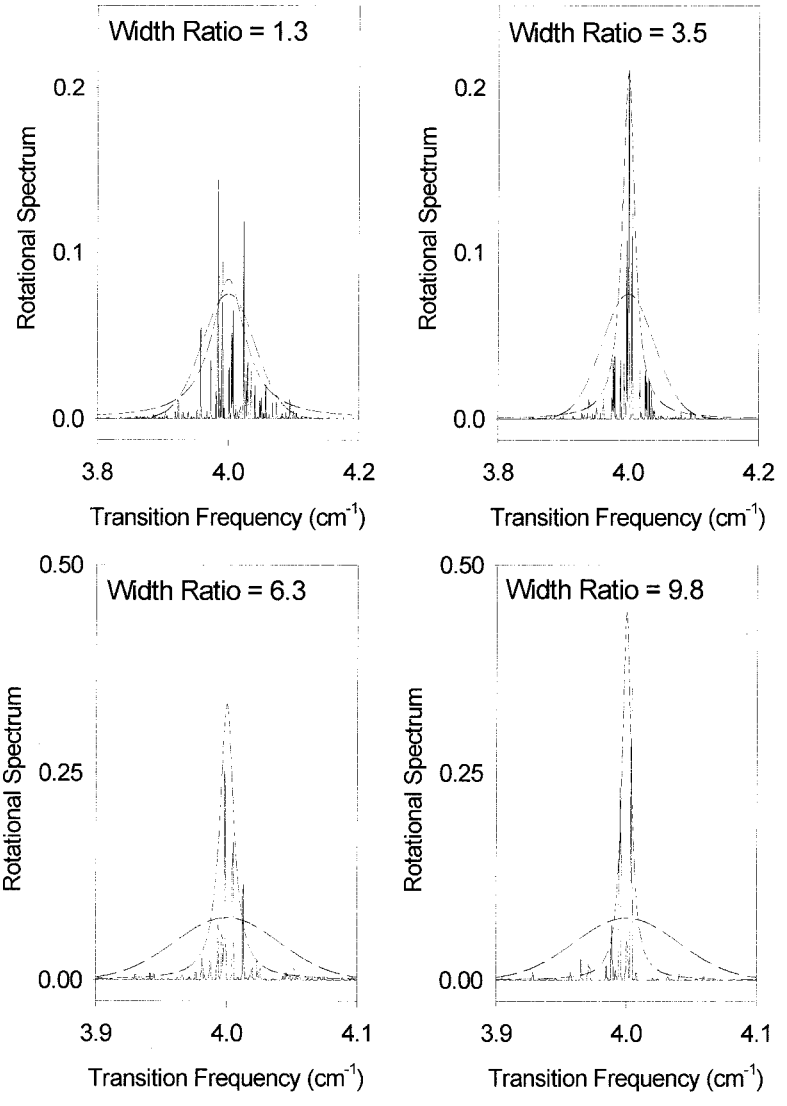

Figure 9. In this figure, the vibrational coupling strength is further increased from the final values of figure 7. As the coupling strength increases, the IVR rate exceeds the dephasing rate determined by the spread of rotational frequencies in the zeroth-order basis (see equation (2.13)). This leads to IVR exchange narrowing of the spectrum. The zeroth-order frequency distribution is described by the Gaussian line shape profile in each panel. The extent of narrowing is given by the width ratio which is the ratio of the IVR rate to the rotational dephasing rate. The overall line shape profile of the rotational spectrum is well described by a Lorentzian curve with a width given by equation (2.13) as shown in each panel.

a 'wobbly' rotational motion and the spectrum evolves to the Gaussian profile determined by the zeroth-order frequency distribution. However, as the sampling (i.e. IVR) rate increases, the molecule rapidly moves between the frequencies of this distribution. For very fast 'IVR exchange' the rotational motion can only pick up the 'average' geometry of the molecule and the rotational motion becomes 'smooth' again at this average frequency. The more regular rotational motion produces a frequency spectrum with a narrower width.

These basic features of the rotational spectroscopy of a molecule in the presence of IVR have been experimentally demonstrated in our measurements on propargyl alcohol [75, 76]. One interesting feature of this measurement is that we can determine the IVR rate by two separate measurements: through the vibrational bright-state spectrum [75] and through the single eigenstate rotational spectrum [76]. We observe different IVR rates, and different dependence of these rates on the angular momentum quantum numbers, through the various techniques. This discrepancy points out a fundamental difference between the two approaches. The vibrational measurement provides a mode-specific IVR rate for a single zeroth-order state (the infrared active bright state). However, in the rotational measurement we start from a molecular eigenstate with a 'microcanonically averaged' vibrational motion. The rotational measurement provides information about the 'average' vibrational dynamics in the energy range and is, therefore, complementary to the vibrational measurement. Studies of this type provide a unique opportunity to determine whether the mode-specific dynamics of the bright state are reflective of the average dynamics occurring in the same energy range.

Finally, we mention some limitations of the current model. Most importantly, we have assumed that the interaction matrix elements between the zeroth-order vibrational states are independent of the total angular momentum (J). However, high-resolution infrared spectroscopy studies of IVR indicate that Coriolis interactions are a common feature of the vibrational state-mixing [21, 23, 72]. For 'perpendicular' Coriolis coupling the matrix elements are J-dependent [14, 15]. This effect leads to a third term in equation (2.7) that will also drive vibrational energy redistribution in the rotational spectroscopy and add an additional lifetime broadening to the spectrum. Quantitative analysis of these effects is currently under investigation in our laboratory. A second omission in this formulation is off-diagonal (in the zeroth-order vibrational basis) vibration–rotation interactions [15]. For molecules with a single stable conformation these terms are expected to be small. However, they may make sizable contributions to cases where isomerization can occur in the energy region being studied [77, 78, 79]. The role these terms play in isomerization processes in energy regions where there is extensive IVR requires further investigation. Empirically, we have not observed the strong rotational-dependence of isomerization rates that would accompany these interactions suggesting they are also weak in the case of large-scale nuclear rearrangement.

3. Conformational isomerization and rotational spectroscopy

In this section, the discussion of the rotational spectrum of a highly mixed quantum state is extended to the case where a molecule can isomerize [62]. In particular, we focus on isomerization about single bonds, a process often called conformational isomerization. Rotational spectroscopy has long played an important role in the understanding of conformational isomerization [80, 81, 82, 83, 84, 85]. Some of the first measurements to demonstrate the presence of distinct molecular

geometries were performed using the standard techniques of microwave spectroscopy [2, 80, 81, 82, 83, 84, 85]. Measurements of the rotational spectra of torsionally excited states has been used to determine the shape of the torsional potential for isomerization [2] (although measurements of the transition frequencies between torsional excited states in the far infrared spectral region have provided a more direct method [86, 87]). The extension of rotational spectroscopy measurements to highly mixed quantum states with energies above the barrier to isomerization permits the determination of the microcanonical isomerization rate and opens a new vista for this traditional technique.

3.1. *Zeroth-order description of the interacting states*

The starting point for understanding the rotational spectroscopy of isomerizing systems is the zeroth-order picture of the quantum states shown in figure 4. In the absence of vibrational state-mixing, the quantum states of the molecule can be approximated as direct products of a small-amplitude wavefunction for the normal-mode motion, a torsional wavefunction obtained from solution of the time-independent Schrödinger equation using the isomerization potential, and an asymmetric top rotational wavefunction. For the case of a single torsional coordinate, the solutions to the Schrödinger equation can be obtained through the usual matrix methods [88].

When the wavefunctions for the torsional Hamiltonian are examined, they can be grouped into two distinct classes [9, 89, 90]. For solutions below the barrier to isomerization, the probability distribution tends to be localized in the distinct wells associated with each conformer. For these quantum states we can assign the conformational structure. Above the barrier to isomerization, the probability distribution tends to be delocalized over the full range of torsional angles. We call these zeroth-order quantum states 'structurally delocalized'. It is, in general, no longer possible to associate a well-defined geometry with these quantum states. For energies well above the barrier to isomerization, these wavefunctions correspond to nearly free-rotor motion in the torsional coordinate.

The model used in figure 4 is essentially the same as the state description typically used to describe unimolecular reactions [5, 6]. In the standard approach, it is convenient to describe above-barrier quantum states as vibrational states of the transition state. For isomerization reactions where there is a well-defined barrier, the transition state corresponds to the molecular structure at the top of the barrier. In the derivation of the microcanonical rate constant in RRKM theory it is common to introduce the motion in the reaction coordinate of the transition state as a particle-in-a-box problem (the size of the box ends up dropping out of this calculation) [5]. This motion corresponds to the 'isomerization' event.

The remnants of this construct can be seen in the torsional wavefunctions. The probability distributions for the first two wavefunctions above the two barriers to isomerization in 4-chlorobut-1-yne are shown in figure 10. When the total energy of the quantum state is only slightly above the barrier to isomerization, the torsional wavefunction has a probability 'build-up' at the transition state geometry. Physically, in the region of the barrier the torsional kinetic energy is very low so that, on average, this is the most likely region to find the system. In a physical sense, spectroscopy of this zeroth-order quantum state would be 'spectroscopy of the transition state'. Since these zeroth-order states will contribute to the highly mixed quantum states as discussed below, we are able to use rotational spectroscopy to 'see the transition state'.

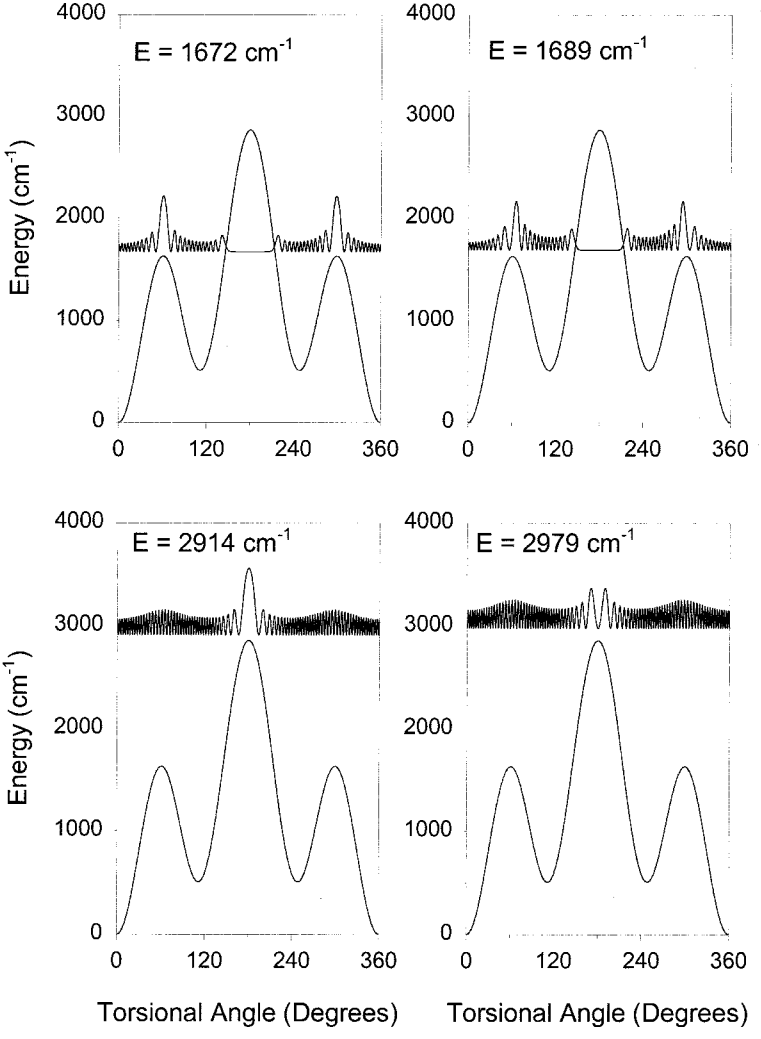

Figure 10. The probability distributions for the first two torsional wavefunctions above the isomerization barriers of 4-chlorobut-1-yne are shown. For energies just above the barrier, the probability distribution is peaked at the transition state structure. The nodal patterns in the region of the transition state are simple (especially for the higher isomerization barrier) and are reminiscent of the particle-in-a-box construct often used to derive the RRKM theory result for the microcanonical rate constant.

When the barrier to reaction is much higher than the typical vibrational frequencies of the molecule, the model described by figure 3 looks more like traditional models for unimolecular reactions as shown in figure 11. The basic physical principles in our model are the same as those used for the statistically adiabatic channel model [91, 92, 93, 94, 95]. Furthermore, if the isomerization barrier is very high, there will be many wavefunctions for the motion in the reaction coordinate that exhibit the 'probability build-up' at the transition state structure. By contrast, only a few of the above-barrier quantum states for low barrier isomerization actually show significant localization at the transition state geometry.

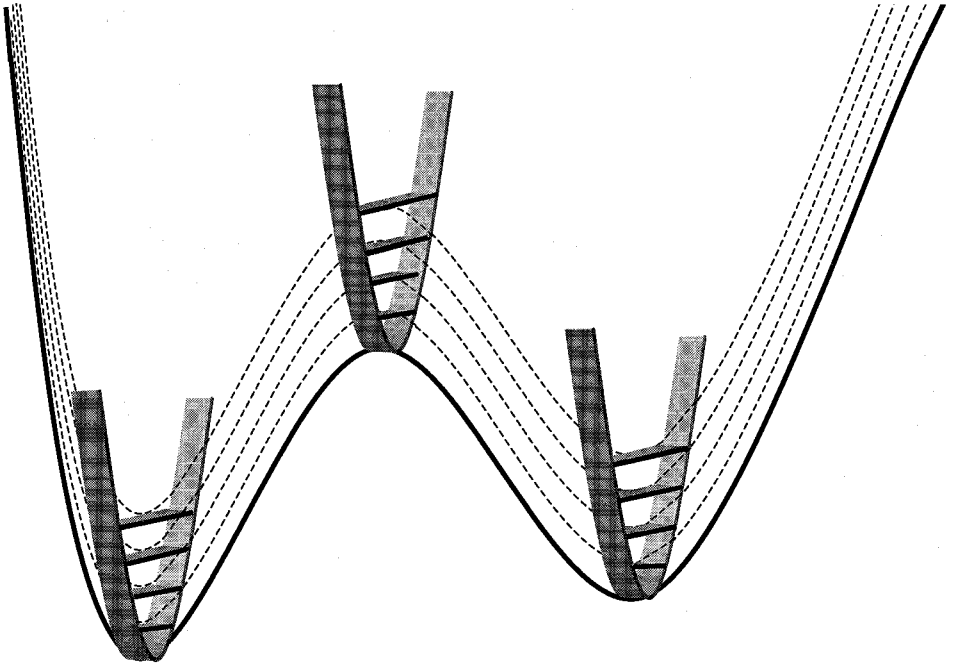

Figure 11. For conformational isomerization reactions, the barrier to reaction is on the same order as the normal-mode vibrational frequencies. In this case, we use the model depicted in figure 3 to describe the spectroscopy and dynamics. If the barrier to reaction is much higher than the vibrational frequencies, the model of figure 3 would appear as shown in this figure where there is an adiabatic torsional potential shown for each vibrational level of one of the normal-modes. This picture resembles the usual descriptions used in RRKM theory and the statistically adiabatic channel method.

This behaviour occurs because the above-barrier energy spectrum for the quantized torsional motion has energy level spacings that are appreciable to barrier height. The torsional wavefunctions rapidly approach the 'smooth' probability profiles expected of a free-rotor solution. In the case of low-barrier conformational isomerization reactions, it is unclear that introducing the 'transition state' is a useful concept.

3.2. *Spectroscopic properties of the zeroth-order states*

To describe the rotational spectrum of molecules undergoing isomerization it is necessary to know the physical properties of the zeroth-order basis states that affect rotational motion. There are two properties that are required: (1) to calculate the frequencies of transitions we need the rotational constants for each basis state and (2) to calculate the transition intensities we need the dipole moment for each basis state. For the case where a molecule can isomerize, the values of the rotational constants and dipole moments will be characteristic of the conformational geometry. This idea forms the basis of using pure rotational spectroscopy to study conformational geometry [2]. The structure of the molecule is, in turn, related to the torsional wavefunction probability distribution for the zeroth-order state. Because the torsional motion can involve the large amplitude motion of a heavy atom, we assume that

the important properties of the zeroth-order states are dominated by the torsional wavefunction. In our study of the rotational spectrum of propargyl alcohol, where there is no large amplitude motion of a heavy atom, we have observed very small changes in the rotational constants (0.4% change) supporting this assumption [76].

In our work, we estimate the rotational constants through the expectation value of the rotational constant over the torsional wavefunction [67, 68, 96]. We obtain the torsional dependence of the rotational constant through a series of single point energy minimizations using standard *ab initio* methods. In a similar manner, we determine the dipole moment for each torsional state. We have tested this method for molecules where the rotational constants of thermally populated excited torsional states have been reported and get good agreement, in general [89, 90, 87]. This approach neglects the Coriolis contribution to the rotational constant, which may be substantial for closely spaced torsional levels. The addition of these contributions will be a later refinement to our analysis.

From the rotational constants for each torsional state it is possible to predict the changes in rotational frequency associated with torsional excitation. An example of this type of calculation is shown in figure 12. We find the same general features in all systems [9, 90]. There are three characteristic sets of frequencies for the torsional states. The highest and lowest frequencies come from torsional states localized in the different stable conformer wells. As the energy of the torsional state exceeds the barrier to isomerization there is a rapid transition to an intermediate frequency. As described above, this region can be roughly thought of as the characteristic rotational frequency of the transition state. The rapid transition between the different characteristic frequencies makes rotational spectroscopy particularly well suited for measuring isomerization rates.

3.3. *Statistical properties of the highly-mixed quantum states*

To introduce dynamics into the problem we must include the interaction terms in the Hamiltonian that couple the zeroth-order basis states. A major goal of our work is to understand the physical origin of these terms so that we can uncover the mechanism for isomerization. This development will require an extensive interplay between theory and experiment and is still in its infancy in our group. In this description of the spectroscopy, we just introduce these interactions empirically. Through some of our studies we have evidence that the dominant interactions occur between the delocalized and the localized states with little evidence for direct interactions between torsional states localized around different geometries [9, 90]. In other words, interactions that lead to 'over-the-barrier' motion are preferred over 'tunnelling' interactions. In any case, if isomerization occurs an effective interaction is implied between zeroth-order states whose torsional wavefunctions are localized in the different conformational minima of the potential. As a result, a single eigenstate of the full Hamiltonian can be represented as a combination of zeroth-order states with torsional wavefunctions that are both localized (around both structures!) and delocalized (over-the-barrier states).

It is possible to proceed with the discussion along the lines of the previous section. In that case, the rotational spectrum for molecules with a single stable geometry could be described in terms of the quantum mechanical average and uncertainty of the rotational constant (with the 'motional' effects of IVR added later). However, for this problem the above approach, which is still valid, obscures the basic features of the spectrum. In this case, it is preferable to treat the three

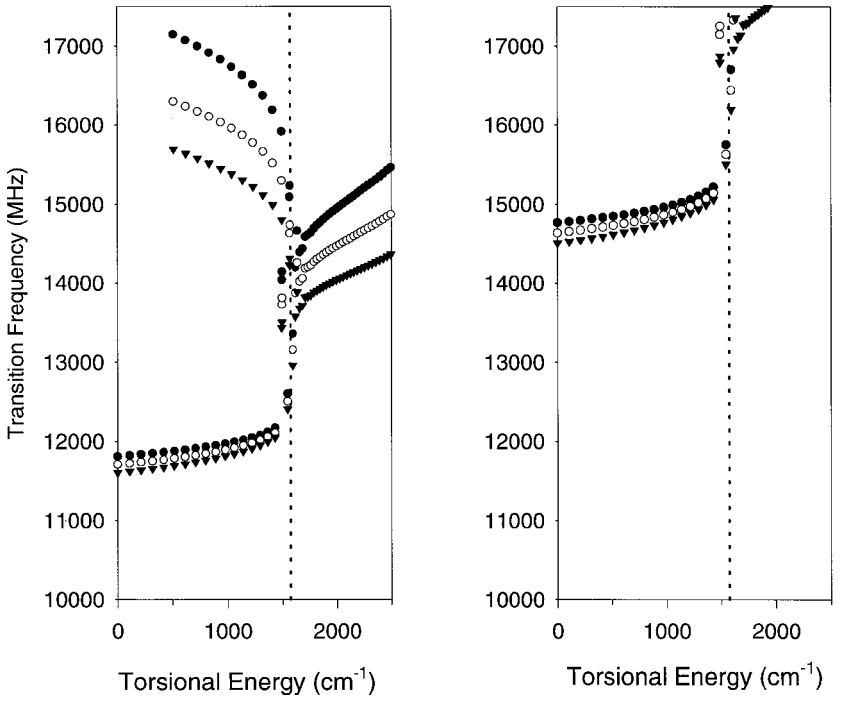

Figure 12. The rotational frequencies for the different torsional states of 4-chlorobut-1-yne are predicted. The rotational constant for each torsional state is estimated through the average of the rotational constant over the torsional wavefunction. The predictions for the $J = 4 \rightarrow J = 3$ transition frequencies are shown on the left. Because the molecule is an asymmetric top, we have indicated the upper (● 4_{13}–3_{12}) and lower (▲ 4_{14}–3_{13}) ranges for the rotational frequency. The centre values are for the predicted 4_{04}–3_{03} asymmetric top rotational transition. The lower frequencies (near 12 GHz) are for the *trans* conformer, which is much closer to the prolate symmetric top limit than the *gauche* conformer (upper frequencies near 16 GHz, larger asymmetry spread). The vertical dotted line indicates the barrier to *trans–gauche* isomerization. Above the barrier, a third characteristic type of rotational frequency (with a sizable vibration–rotation interaction term as indicated by the slope) emerges. These frequencies can be identified with the transition state geometry. On the right, the $J = 4 \rightarrow J = 5$ predicted transition frequencies are shown. Only rotational frequencies of the *trans* conformer (near 14.5 GHz) are expected to fall in our experimental range (10–17.5 GHz). Notice that the $J = 4 \rightarrow J = 5$ *trans* frequencies are expected to occur near the $J = 4 \rightarrow J = 3$ *gauche* transitions. This behaviour makes it necessary to be able to experimentally determine the sign of the transition frequency.

distinct contributions to the structurally mixed eigenstates separately [62]. In this way, we can introduce a 'partial probability' for each type of zeroth-order state: states with torsional wavefunctions localized around the more stable conformation (labelled I), states localized around the less stable conformation (labelled III) and states with delocalized wavefunctions (labelled II). In this basis set a single molecular eigenstate can be written as

$$|\phi_j\rangle = \sum_{p=1}^{\text{N\_TypeI}} c_p^{(j)} \left|\, {}^{\text{I}}_{p}\right\rangle + \sum_{q=1}^{\text{N\_TypeII}} c_q^{(j)} \left|\, {}^{\text{II}}_{q}\right\rangle + \sum_{r=1}^{\text{N\_TypeIII}} c_r^{(j)} \left|\, {}^{\text{III}}_{r}\right\rangle. \tag{3.1}$$

For the jth structurally mixed eigenstate, the probabilities of finding the molecule in zeroth-order states associated with the three different torsional properties are defined as

$$\text{Prob\_I}_j = \sum_{p=1}^{\text{N\_TypeI}} \left|c_p^{(j)}\right|^2, \tag{3.2}$$

$$\text{Prob\_II}_j = \sum_{q=1}^{\text{N\_TypeII}} \left|c_q^{(j)}\right|^2, \tag{3.3}$$

$$\text{Prob\_III}_j = \sum_{r=1}^{\text{N\_TypeIII}} \left|c_r^{(j)}\right|^2. \tag{3.4}$$

In each of these equations, the sum runs over the number of zeroth-order basis states of each individual type. By completeness, the total probability is one. In the case of 'complete mixing' these three probabilities will be the same for all molecular eigenstates and will simply be the fraction of states of each type at the energy of interest. This relationship can be expressed in terms of the state-densities for the zeroth-order states as

$$\text{Prob\_I} \rightarrow \frac{\rho_{\text{TypeI}}}{\rho_{\text{TypeI}} + \rho_{\text{TypeII}} + \rho_{\text{TypeIII}}} = \frac{\rho_{\text{TypeI}}}{\rho_{\text{total}}} \tag{3.5}$$

with similar expressions for the other two types of zeroth-order quantum states. In terms of a standard chemistry interpretation, these probabilities are simply the microcanonical 'concentrations' of the three types of states. Because we are considering the properties at a fixed total energy of the molecule, these relative concentrations depend both on the relative stability of the conformers (ΔH-like term) and the vibrational frequencies of the two conformers (ΔS-like term). The ratio of the populations is simply related to the microcanonical equilibrium constant at the energy (ΔG-like term).

However, there is an important distinction between the quantum view of the isomerization reaction and the simple chemistry view. In a classical view of this chemical reaction, we would think of an ensemble of molecules where there is a mixture of molecules with different structures, say the reactant, product and (with a fleeting existence) the transition state. (Note that this is the same view given by the zeroth-order basis.) However, in reality the ensemble consists of a set of molecules where each individual molecule is product, reactant and transition state simultaneously. (This view is the molecular eigenstate picture.) In terms of the torsional wavefunction for an eigenstate of the full Hamiltonian, there will be probability of finding the system in all of the different conformational geometries. An example of a structurally mixed eigenstate is depicted in figure 13 from model calculations of the isomerization dynamics of 4-chlorobut-1-yne.

3.4. *The rotational spectrum of a structurally mixed quantum state*

At the simplest level, the rotational spectrum for a structurally mixed quantum state is expected to show rotational transitions at the different characteristic frequencies of the molecule: the frequencies associated with states localized around each stable conformer geometry and with the frequency characteristic of the delocalized

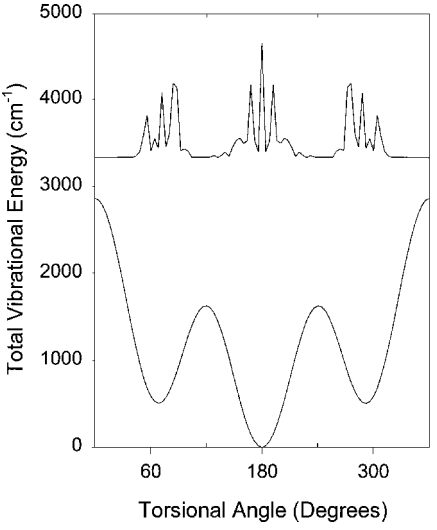

Figure 13. This figure depicts a 'structurally mixed' eigenstate of 4-chlorobut-1-yne near 3330 cm^{-1}. The wavefunction was calculated through a random matrix calculation that models the observed isomerization rate (see section 4). The probability distribution of this single eigenstate contains contributions from both the *trans* (more stable) and *gauche* (less stable) conformations.

torsional states (see figure 14). In other words, each part of the wavefunction is expected to project out its characteristic spectrum. In this way, we can obtain structural information about the different stable conformations, as well as the transition state in favourable cases, from the spectrum of a single quantum state. However, as in the case for molecules with a single stable geometry, the dynamics of the system play an important role in determining the overall line shape profile of the single eigenstate rotational spectrum.

For the rotational spectrum of a molecule undergoing isomerization there are two different types of dynamics that need to be considered. First of all, there are interactions that lead to vibrational energy flow between states of the same geometry. The effects of these dynamics have been presented in the previous section. Secondly, there are interactions between states of different torsional character. Based on previous experimental evidence, we assume that interactions occur between states of each conformer and the delocalized torsional states (direct interactions between torsional states localized around different stable geometries are assumed to be much weaker). By analogy with the standard NMR notation, the first type of interactions lead to dynamics on a time scale that will be denoted T_2. These dynamics maintain conformational structure and, therefore, do not contribute to the lifetime of the isomer. The second type of interactions lead to a dynamical time scale that will be denoted T_1 [3, 97]. In this case, the interactions lead to the decay of probability for the stable geometry and, therefore, determine the lifetime of the conformer.

The actual values of T_1 and T_2 for each conformer can be obtained from the Hamiltonian. In the case where there are three characteristic types of torsional states

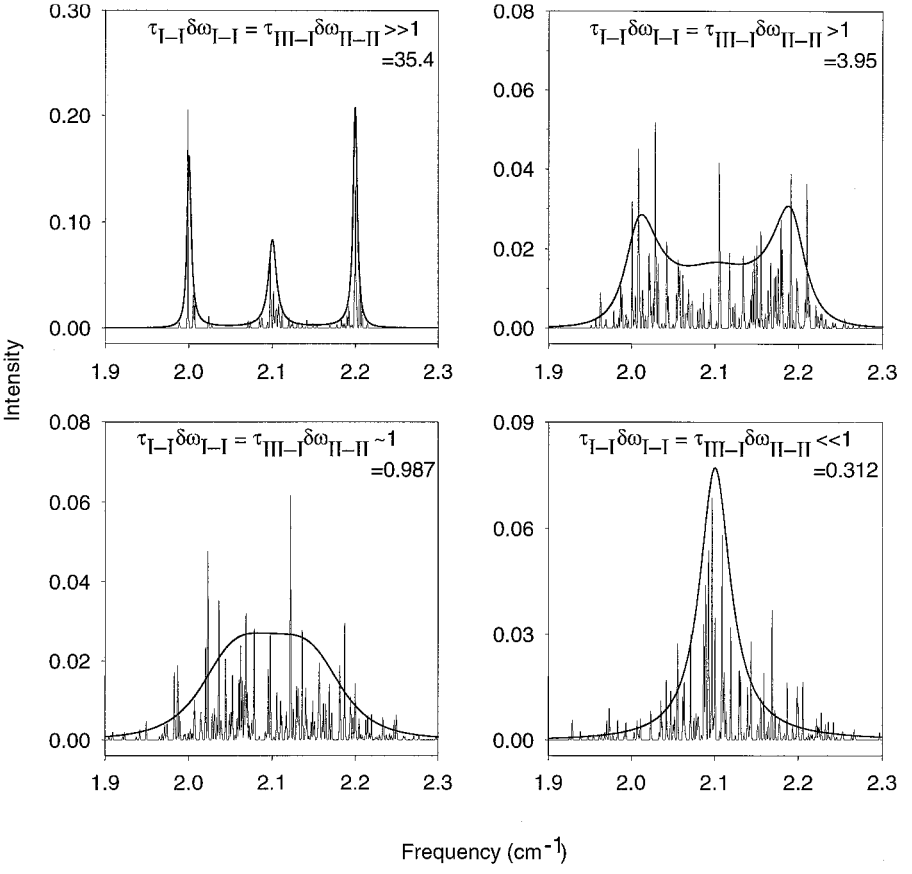

Figure 14. Model calculations of the single eigenstate rotational spectrum for a molecule undergoing isomerization are shown as T_1 is decreased (equation (3.7)). In this model, there are equal densities of three different types of torsional states (e.g. the *trans*, *gauche* and delocalized states of figure 3). Each characteristic torsional state has a separate average rotational frequency (see figure 12). For slow isomerization, upper left, the rotational spectrum of a single eigenstate shows all three characteristic frequencies. As the isomerization rate increases, the overall line shape profile of the spectrum undergoes coalescence. Eventually, for very fast isomerization, a single peak is observed at the average rotational frequency of the coupled states (bottom right panel). The solid line that describes the line shape profile is calculated from the Bloch model modified for exchange that is commonly used to interpret NMR coalescence spectra.

[98], the Hamiltonian can be written in the following block form

$$H = \begin{pmatrix} H_{\mathrm{I}} & W_{\mathrm{I-II}} & 0 \\ W^{*}_{\mathrm{I-II}} & H_{\mathrm{II}} & W_{\mathrm{II-III}} \\ 0 & W^{*}_{\mathrm{II-III}} & H_{\mathrm{III}} \end{pmatrix}. \tag{3.6}$$

Each entry in this Hamiltonian is itself a matrix. For example, the entry H_{I} includes all zeroth-order states of structure I and the interactions between these states (i.e. it has the form of equation (1.1)). The two interaction blocks (W) describe the

coupling between the states localized around the two stable conformations (I and III) with the states that have above-barrier torsional wavefunctions (II).

To illustrate the basic properties of the rotational spectroscopy of a single eigenstate of the Hamiltonian given in equation (3.5), we use a random matrix model. In this model calculation, it is assumed that the densities of the three types of states are equal. Additionally, we assume that the two interaction blocks are identical. In this case, we can define the T_1 and T_2 times using a Fermi Golden Rule rate expression

$$T_1 = \frac{1}{2\pi\Gamma_{\mathrm{I-II}}} = \frac{1}{2\pi\Gamma_{\mathrm{II-III}}} = \frac{1}{2\pi\left(2\pi\left\langle W^2_{\mathrm{I-II}}\right\rangle\rho\right)}, \tag{3.7}$$

$$T_2 = \frac{1}{2\pi\Gamma_{\mathrm{I-I}}} = \frac{1}{2\pi\Gamma_{\mathrm{II-II}}} = \frac{1}{2\pi\Gamma_{\mathrm{III-III}}} = \frac{1}{2\pi\left(2\pi\left\langle W^2\right\rangle\rho\right)}, \tag{3.8}$$

where $\langle W^2\rangle$ is the root-mean-square d interaction matrix element between states of the same structure (assumed identical for all three types of states) and ρ is the density of states for each structure.

The effects of the coupling between states of the same conformer are similar to those described above. As the interaction matrix elements between states of a given conformation increase (T_2 decreases), there is a narrowing of the characteristic spectrum for that conformation. For the conformational isomerization problem there can be significant 'inhomogeneous' broadening of the conformer spectrum that comes from the contributions of highly excited torsional states. For example, the rotational frequencies for the gauche conformer of chlorobutyne show a wide dispersion in figure 14. Additionally, through interactions that mix the value of the K_a rotational quantum number, there will be an additional width contribution from the molecular asymmetry. Fast IVR within a conformational structure can serve to reduce these inhomogeneous effects in the spectrum through the IVR exchange mechanism.

The variation in the single eigenstate rotational spectrum as a function of the T_1, with fixed T_2, is shown in figure 14. The overall line shape profile for the spectrum (solid line) is calculated from the Bloch model modified for chemical exchange using the T_1 and T_2 values given in equations (3.7) and (3.8) [97]. For slow isomerization the spectrum shows the 'simple' appearance expected for the structurally mixed quantum state. From a single quantum state we can obtain the spectrum of each conformer and the delocalized states. As the isomerization rate is increased, by increasing the interaction matrix elements between the stable conformers and the delocalized states, the line shape undergoes coalescence [99, 100, 101]. At first, there is simply a broadening in each of the three characteristic frequency regions. In accord with the NMR nomenclature, this broadening simply reflects the shortening of the lifetime of the geometry (T_1). In this regime, the isomerization rate can be estimated from the line width of the spectrum. However, this provides only an upper limit to the rate because there is also the T_2 line width contribution to the spectrum. This limitation is common to frequency-domain methods for determining dynamics. As the interaction strength is further increased, the maxima of the spectra shift towards the average frequency. For sufficiently fast isomerization (short T_1), the rotational spectrum appears as a single peak at the average frequency position. Further increases of the rate will lead to additional *narrowing* of this spectral feature.

This evolution of the line shape can be understood on classical grounds. Consider the general physics example of an ice skater executing a spin with arms either extended or close to the body. Because the total angular momentum of the skater is conserved, there will be two characteristic rotational frequencies for the spinning motion. Now, let the skater start 'isomerizing' by alternating their arm position. If this alternation is sufficiently slow, we can perceive the two separate frequencies. However, if the alternation is rapid, a single, average frequency will begin to emerge. Even faster alternation, compared to the time scale of the rotation, will lead to a 'smooth' rotational motion composed of a narrow range of frequencies. This classical picture provides a good description of the physics of coalescence and narrowing of the rotational spectrum of an isomerizing molecule.

For the case where we can observe all three characteristic spectra, the isomerization is sufficiently slow that the geometry is maintained long enough to define each frequency. In particular, we can interpret the intermediate frequency as the rotational motion as the molecule passes over the barrier, i.e. while it has the transition state structure. If the barrier passage is slow, the molecule has time to rotate as it converts between the two stable geometries and this frequency is well-defined in the spectrum. When the isomerization is too fast to permit rotation in each characteristic geometry, we loose the ability to define precise frequencies for each shape. The time scale that defines this break point is related to the *differences* between the characteristic frequencies. This fact offers a convenient method for 'resolving' the frequencies for each geometry. Because the rotational frequency differences scale linearly with the total angular momentum, this 'break point' can be varied by studying different rotational transitions. For example, if the spectrum has entered the coalescence regime at low J, the three frequencies can be resolved by measuring a higher rotational transition. This idea is illustrated in figure 15 [98]. The ability to change the characteristic time scale for coalescence is a feature that does not exist for NMR spectroscopy where the chemical shifts of the two species are not easily varied.

In summary, the isomerization kinetics of the molecule at a well-defined energy can be obtained from the line shape of the rotational spectrum of a single quantum state. In this way, the microcanonical rate constant ($k(E, J)$) can be measured directly [5, 6]. The required spectroscopic parameters for simulating the line shape can be obtained from the torsional eigenfunctions and *ab initio* calculations. In section 4 of this review, this approach will be illustrated for the case of 4-chlorobut-1-yne.

3.5. *Time-domain interpretation of the spectroscopy*

Finally, we discuss the connection between the observed spectrum and the isomerization kinetics. In particular, we would like to tie together the Hamiltonian dynamics, the classical kinetics approach of chemistry and the spectroscopy of a structurally mixed quantum state. For simplicity, we now restrict ourselves to a problem with only two characteristic geometries (now labelled I and II) and we omit consideration of the above-barrier wavefunctions. As a starting point, consider the standard kinetics approach to describing the isomerization reaction between these two conformers

$$\mathrm{I} \underset{k_{-1}}{\overset{k_1}{\rightleftharpoons}} \mathrm{II}. \tag{3.9}$$

A common method for measuring fast chemical kinetics uses relaxation techniques [102]. In these methods, the reaction is initially at equilibrium. A perturbation

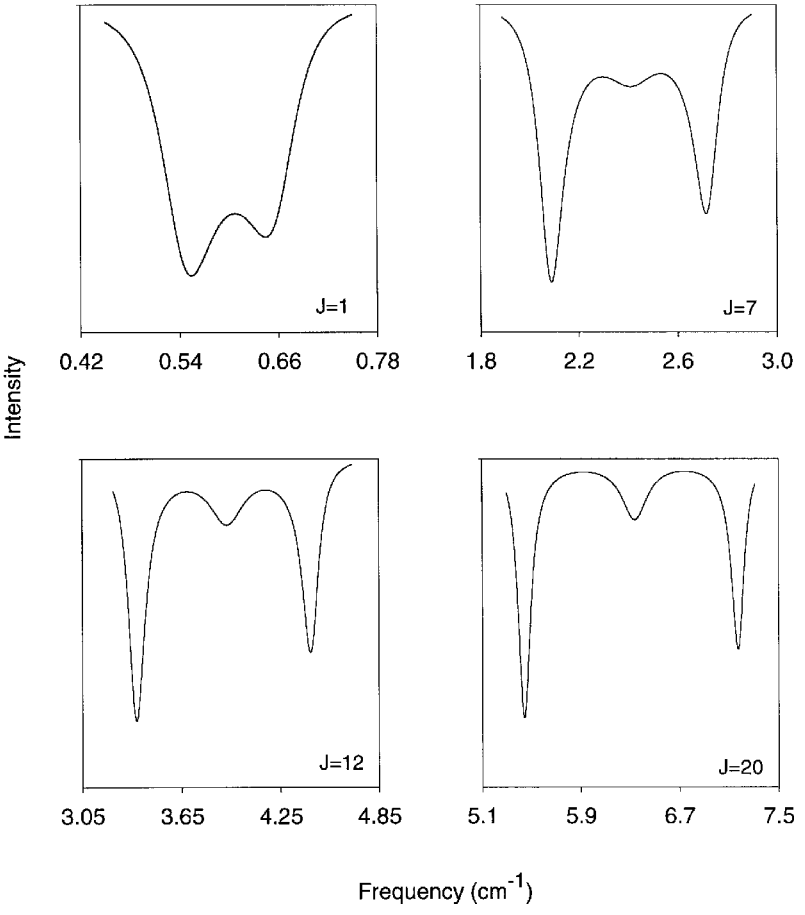

Figure 15. The coalescence phenomenon (see figure 14) occurs when the isomerization rate (T_1^{-1}) exceeds separation of the characteristic rotational frequencies. For rotational spectroscopy, the frequency separation scales linearly with the total angular momentum, J. Therefore, for a fixed isomerization rate, the spectrum can be brought out of coalescence by measuring the rotational spectrum at larger values of J. This effect is illustrated by showing the calculated J-dependent line shape profiles (from the Bloch model, see figure 14) for a fixed rate isomerization process. Physically, the molecule must rotate a few cycles with a given structure for that frequency to be defined in the spectrum. At a fixed rate of barrier passage (i.e. isomerization), we can sample the transition state structure by going to a rotational energy where the characteristic time scale for rotation is faster than the time for passing over the barrier. The 'spreading' of the spectrum permits resolution of the rotational frequencies associated with the transition state geometry which are initially obscured by coalescence.

is rapidly applied that removes the system from equilibrium and the time needed to reestablish the initial state is determined. For the model first-order isomerization reaction the measured relaxation rate will be the sum of the forward and reverse rates

$$k_{\text{obs}} = k_1 + k_{-1}. \tag{3.10}$$

We now show that the single eigenstate rotational spectroscopy technique is analogous to relaxation techniques.

First of all, we point out that we can think of a 'fully mixed' quantum state as an equilibrium situation. Specifically, the quantum state is a solution to the time-independent Schrödinger equation and is, therefore, stationary. Furthermore, if we use the definitions of total probability as defined in equations (3.2)–(3.4), then the ratios of the Type I and Type II probabilities in the quantum state will simply reflect the microcanonical equilibrium constant of the reaction.

To take the quantum state out of equilibrium we can apply a pulse of radiation. In particular, consider the case where the rotational spectrum of the eigenstate has Type I and Type II resolved spectra (as illustrated in figure 15, this can be achieved by going to a higher rotational transition if necessary) [62]. Furthermore, let the frequency spectrum of the light pulse cover only one characteristic region of the spectrum (say, Type I). Because the rotational spectrum extends over several molecular eigenstates, the light pulse will create a superposition state. This superposition state will then undergo 'kinetics' and evolve in time. With regards to the isomerization reaction, we are interested in the structural properties during this time-evolution.

To quantify the structural properties of the time-evolving superposition state we use the probability definitions defined in equations (3.2)–(3.4). In relation to chemical kinetics, these probabilities behave as the concentration. To follow the isomerization reaction, these 'concentrations' are calculated as a function of time by the following prescription

$$\mathrm{Prob\_TypeI}(t) = \sum_{p=1}^{\mathrm{N\_TypeI}} \left| \left\langle {}^{\mathrm{I}}_{p} \right| \Psi(t) \right\rangle \Big|^2. \tag{3.11}$$

An analogous expression can be written for the time evolution of the total probability of finding the molecule in a zeroth-order basis state that has structure II. The results for the two-structure model are shown in figure 16 [62]. When the light pulse can differentiate between the two structures, the initial superposition state is localized in a single structure. The light pulse has 'projected out' a single structure from the mixed state. However, structure localization is not an 'equilibrium' condition and we find decay of the probability back to the initial condition as the superposition state 'dephases'. Going back to the model Hamiltonian for the problem, we can define the forward and reverse rates of the reaction using Fermi's Golden Rule

$$k_1 = 2\pi \left\langle W^2_{\mathrm{I-II}} \right\rangle \rho_{\mathrm{II}}, \tag{3.12}$$

$$k_{-1} = 2\pi \left\langle W^2_{\mathrm{I-II}} \right\rangle \rho_{\mathrm{I}}. \tag{3.13}$$

Using these definitions we find that the decay to equilibrium occurs with a rate that is the sum of the forward and reverse rates.

This interpretation of the problem shows how the microcanonical rate constant determined from the rotational spectrum of a single eigenstate can be related to the interaction terms of the Hamiltonian. Furthermore, by appealing to the time-domain picture we can connect the intramolecular dynamics to the usual chemical kinetics picture. However, we should again point out the different view of isomerization that we obtain from spectroscopy. In classical kinetics we would consider that there are two separate populations of molecules that are interconverting. At any given time, each molecule would have either structure I or structure II. However, for the

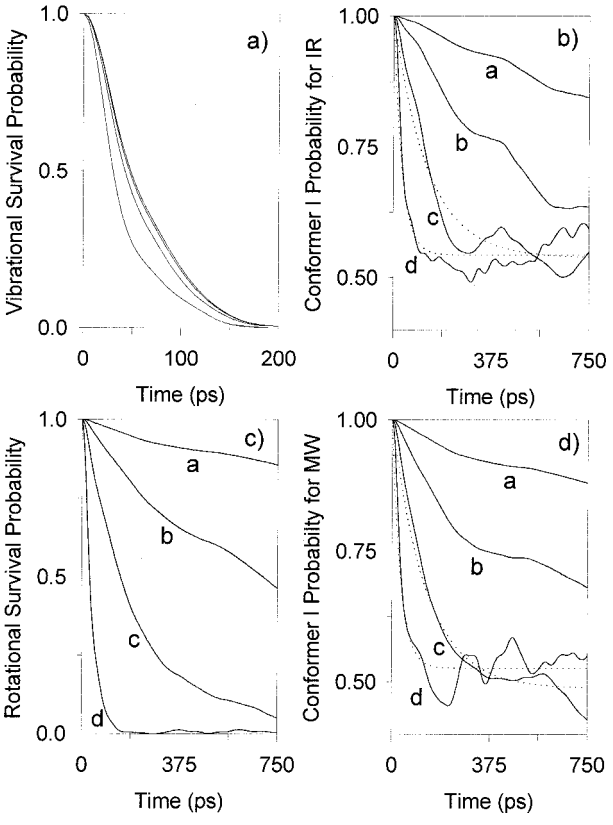

Figure 16. The kinetics for a two-state isomerization problem are presented. The IVR lifetime for interactions between states with the same structure (T_2, equation (3.8)) is set at 60 ps. This lifetime will be observed in the survival probability calculated from the vibrational spectrum (*a*). In the two-state model, there is also a characteristic time scale for energy flow between the structures (T_1, equation (3.7)). In (*b*), the isomerization dynamics following vibrational excitation are determined using equation (3.11) at four different T_1 values (*a–d*). Following bright-state excitation (which has structure I), the total Type I probability decays to the equilibrium value of 0.5. The rate for approaching equilibrium is given by equation (3.10) using the relations of equations (3.12) and (3.13). Simple exponential decay at the sum of the forward and backward rates of isomerization is indicated by the dotted lines in (*b*). Notice that the time scale for isomerization is slower than that for IVR so that there is little change in the vibrational survival probability dynamics. By contrast, the width of the eigenstate rotational spectrum, as measured through its survival probability (*c*), does track the isomerization dynamics (*d*). After coherent excitation of the Type I rotational spectrum, the molecule assumes the Type I structure (the probability of being in a Type I state is unity (panel (*d*)). This probability decays to the equilibrium value of 0.5 on a time scale determined by equation (3.10).

Hamiltonian kinetics we are considering the dynamics of a single molecule. Initially it has neither structure I nor structure II but, in a sense, is a superposition of the two. Through coherence properties, a short light pulse can relocalize the molecular geometry if the spectrum is resolved for the two forms. However, the molecule with well-defined structure above the barrier is not an equilibrium state and this

geometry localization decays at the relaxation time given by the sum of the forward and reverse rates.

4. Applications to kinetics

In this section we present a concrete example of the application of the single eigenstate rotational spectroscopy technique to the problem of conformational isomerization. The example we will use is our recent measurements of *trans–gauche* isomerization of chlorobutyne (4-chlorobut-1-yne) at 3331 cm^{-1} [10, 103]. For this molecule, we find that the microcanonical rate constants are about 800 times slower than predicted by RRKM theory. The violation of RRKM theory for this class of reactions is likely to be common [104, 105]. Therefore, conformational isomerization is a problem where a full dynamical theory is required to describe the kinetics. Finally we conclude this section, and the review, with some comments about the generalization of our method to other forms of spectroscopy and how this can be used to address fundamental problems in kinetics and laser chemistry.

4.1. *An example of conformational isomerization measurements: 4-chlorobut-1-yne*

To demonstrate the features of the rotational spectroscopy of single eigenstates in the case where isomerization occurs, we present our recent results on chlorobutyne [103]. There are no previous reports of the pure rotational or vibrational spectroscopy of chlorobutyne, so our analysis relies extensively on *ab initio* calculations of the molecular structure and vibrational normal-mode frequencies. The one-dimensional (1D) torsional potential for conformational isomerization of chlorobutyne is shown in figure 17. The potential was calculated at the HF/6-31+G** level using Gaussian 98 [106]. At a series of fixed torsional angles, the energy is calculated with geometry relaxation of all other internal coordinates. A number of the torsional energies for the 1D problem are included in the figure 17. These energies are calculated by solving the 1D Schrödinger equation in a free rotor basis set. The internal rotation constant (F) is fit to a Fourier series using the geometries from the *ab initio* calculations [88]. Previous studies of large amplitude torsional motion have shown that current *ab initio* methods provide an accurate description of the spectroscopy [86, 86]. In this potential, the lowest energy structure is the *trans* conformer. This result is in agreement with our molecular beam measurements where we have only been able to observe spectra for this conformation (in both the vibrational and pure rotational spectrum).

From the *ab initio* vibrational frequencies, we can calculate the total vibrational state density of chlorobutyne near the acetylenic C–H stretch fundamental (3331 cm^{-1}). In this calculation, we categorize the quantum states based on their torsional properties using the model shown in figure 4. The distribution of vibrational states near 3331 cm^{-1} is given in table 1. In the high-resolution rovibrational spectrum of chlorobutyne we find that the measured total vibrational state density is close to the total state density listed in table 1. This agreement provides indirect evidence that isomerization, defined as the interaction between the *trans* and *gauche* conformer states, occurs at this energy [107, 108]. Using the *ab initio* vibrational frequencies and the torsional energies from the 1D calculation, we can predict the conformational isomerization rate using the standard formula from RRKM theory: $1 \times 10^{13}\ s^{-1}$ ($\tau_{isom} = 0.1$ ps).

The central portion of the high-resolution infrared spectrum of the predominantly a-type acetylenic C–H stretch spectrum of chlorobutyne is shown in figure 18.

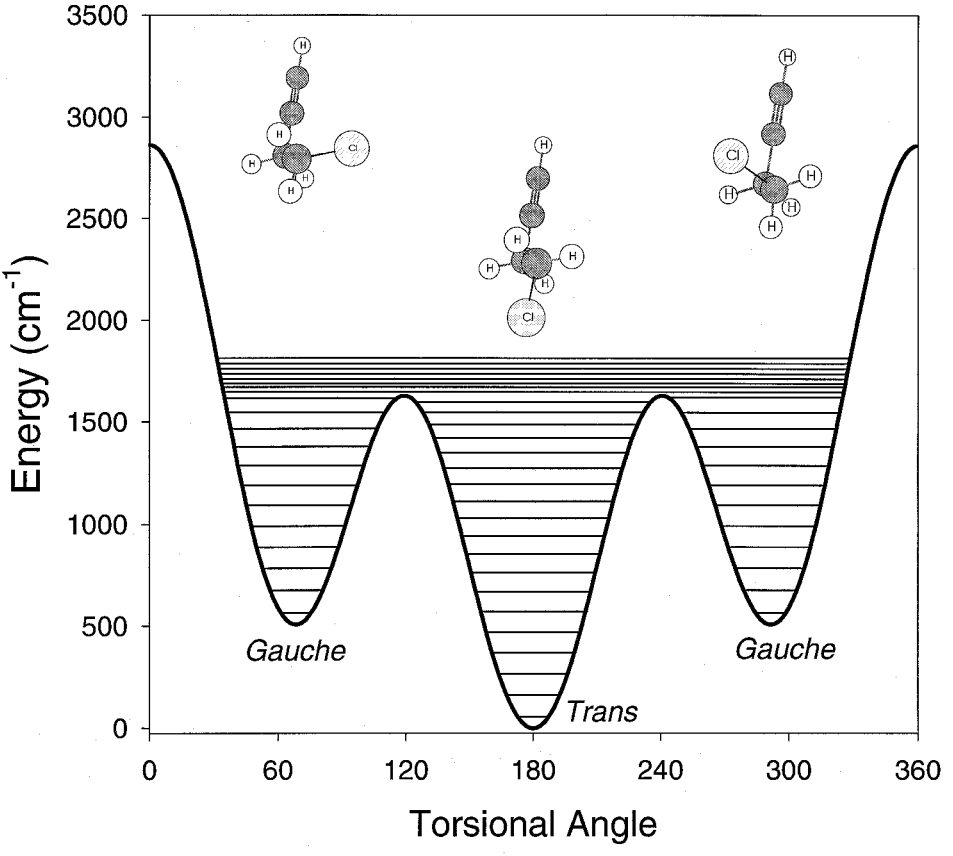

Figure 17. The torsional potential for 4-chlorobut-1-yne, determined by *ab initio* methods, is shown. The torsional energy levels shown on the potential are calculated from the 1D Schrödinger equation for hindered internal rotation. The more stable (*trans*) and less stable (*gauche*) conformations are shown. The barrier to *trans–gauche* isomerization is approximately 1500 cm^{-1}.

Table 1. Density of states at 3330 cm^{-1}.

Trans	89 states cm^{-1}
Delocalized	11 states cm^{-1}
Gauche	59 states cm^{-1}
Total	158 states cm^{-1}
Measured	~ 180 states cm^{-1}

The ground state of this spectrum has the *trans* conformation. Within the model of figure 4, the zeroth-order spectrum involves a transition to the lowest torsional level of the acetylenic C–H stretch adiabatic potential. As a result, the rotational band contour of the spectrum will be characteristic of the *trans* conformation. This effect

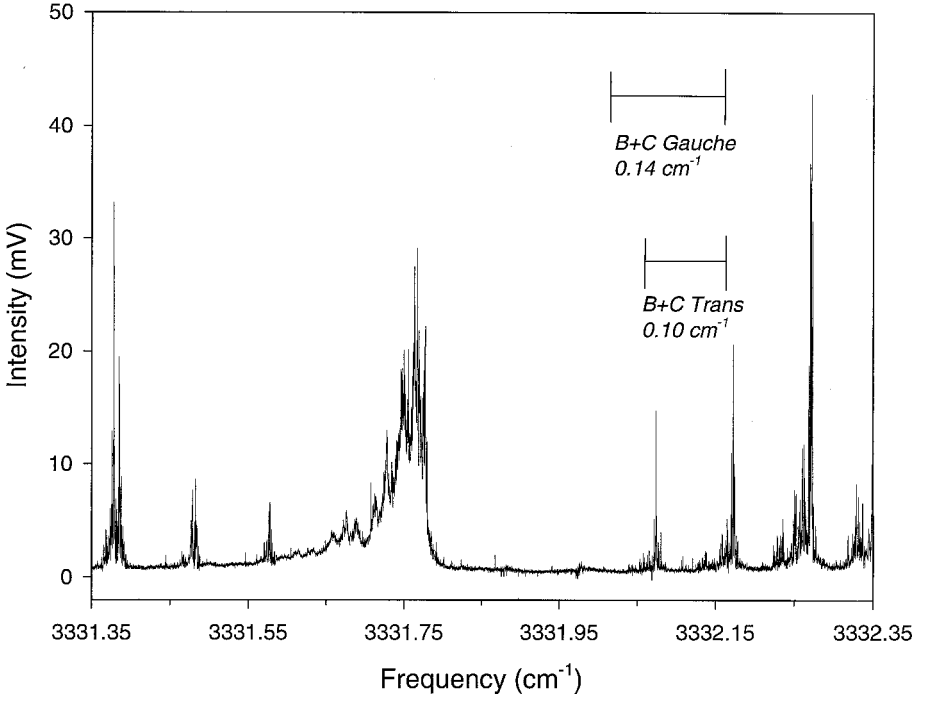

Figure 18. The central portion of the a-type rovibrational spectrum of the acetylenic C–H stretch of chlorobutyne is shown, with the Q-branch occurring at 3331.75 cm^{-1}. The resolution of the spectrometer is 5 MHz (0.0002 cm^{-1}). The rotational fine structure is typical for a near-prolate asymmetric top molecule and has a spacing that matches the rotational constants of the more stable *trans* conformer ($B + C = 0.1\ cm^{-1}$).

is observed through the characteristic P- and R-branch spacings ($B+C$) of 0.10 cm^{-1}. For comparison, this spacing in the *gauche* conformer is predicted to be 0.14 cm^{-1}. The infrared spectrum of chlorobutyne has several types of inhomogeneous congestion that prevent clean excitation of a single eigenstate at the 5 MHz resolution of our spectrometer. These contributions are rotational congestion from the tight level structure of a near prolate asymmetric top, the presence of two chlorine isotopes, and the hyperfine splitting from the chlorine nucleus ($I = 3/2$ for both ^{35}Cl and ^{37}Cl) [1].

Using ground-state microwave-infrared double-resonance spectroscopy we can obtain the high-resolution infrared spectra with rotational, hyperfine and isotope selectivity [8]. Example double-resonance spectra are shown in figure 19. From these spectra we can determine the survival probability for coherent vibrational excitation of the acetylenic C–H stretch *of the trans conformer*. The time scale for the decay of the survival probability, i.e. the rate of IVR, sets an upper limit to the isomerization rate following short-pulse infrared excitation. For chlorobutyne, the IVR rate is approximately $3.3 \times 10^8\ s^{-1}$ ($\tau_{ivr} = 3000$ ps). This rate is 4 orders of magnitude slower than the calculated RRKM rate.

To directly detect the isomerization process we perform rotational spectroscopy on single eigenstates near 3331 cm^{-1}. To prepare single-eigenstates we use upper-state microwave-infrared double-resonance spectroscopy [76]. In these measurements, the

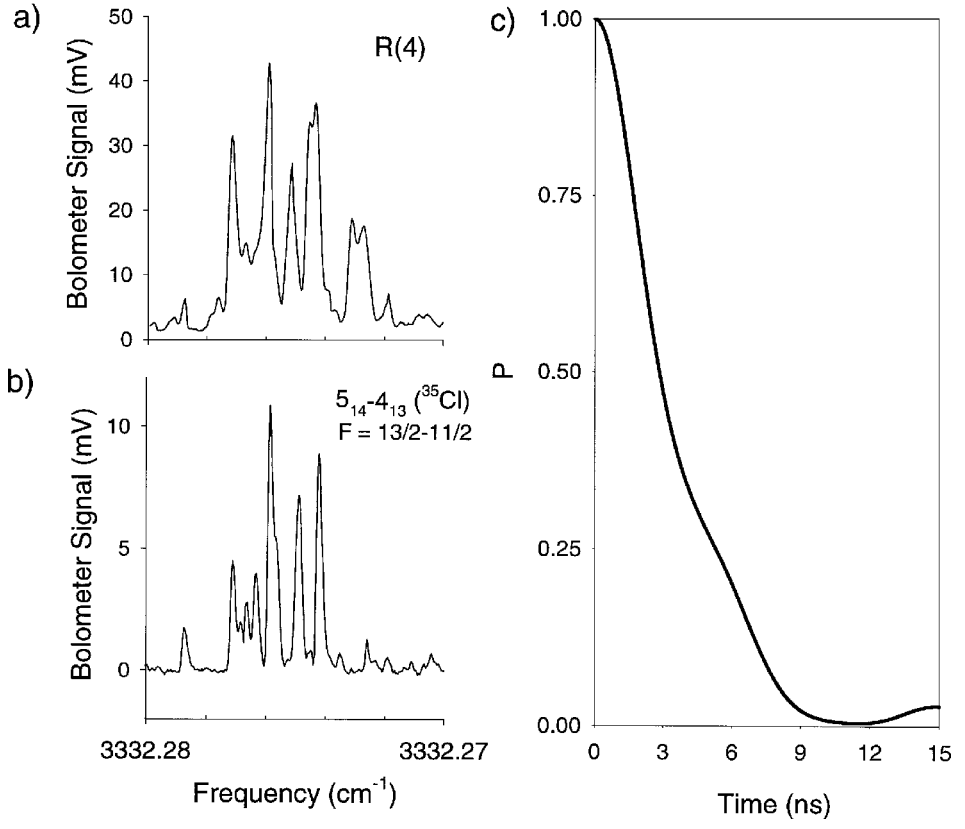

Figure 19. (*a*) The R(4) region of the a-type acetylenic C–H stretch rovibrational spectrum. In this region there is extensive overlap of transitions from different rotational quantum numbers, isotopes, and Cl-hyperfine components. (*b*) Using infrared-microwave double-resonance spectroscopy, the spectrum of a single rovibrational transition (and single isotope and hyperfine component). From this spectrum, the IVR lifetime (3 ns, (*c*)) is determined from the survival probability (equation (1.5)). The IVR rate of the bright state obtained in this measurement provides an upper limit to the conformational isomerization rate following coherent vibrational excitation of the acetylenic C–H stretch of the *trans* conformer.

infrared laser is actively stabilized to a strong absorption feature (which involves the overlap of a few molecular eigenstate transitions). The strongest eigenstate transitions under the infrared line shape can be saturated. An amplitude modulated microwave source is then scanned to produce a double-resonance spectrum with higher frequency resolution (300 kHz). A portion of the double-resonance scan, and comparison to the infrared spectrum in the same energy region, is shown in figure 20. Through this double-resonance excitation, single eigenstates with known total angular momentum quantum number can be prepared.

Finally, using a second, high-power microwave source, the rotational spectrum of the single eigenstate is measured through an infrared–microwave–microwave triple-resonance experiment [10]. One new feature of the rotational spectroscopy of structurally mixed states is the need to determine whether a transition reaches a final quantum state that is higher or lower in energy. For pure rotational spectroscopy this

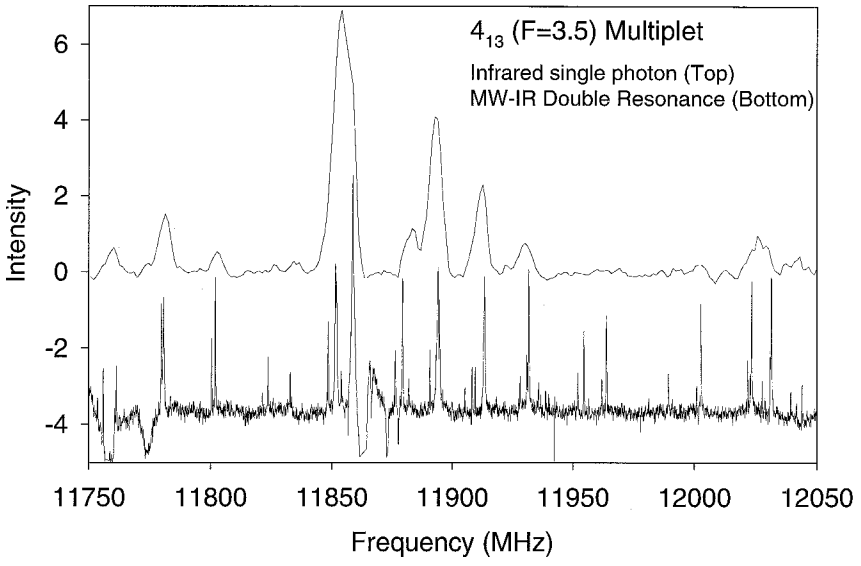

Figure 20. To ensure single eigenstate excitation in the chlorobutyne spectrum, it is necessary to use infrared-microwave double-resonance spectroscopy methods. This figure compares $J = 3 \rightarrow J = 4$ rotational spectrum of the strongest feature in the P(4) spectrum with the infrared spectrum of the $J = 4$ acetylenic C–H stretch bright state (upper trace). The resolution in the double-resonance spectrum is 0.3 MHz compared to the infrared resolution of 5 MHz.

information can be determined based on the rotational spectrum pattern. However, in the case where contributions from different conformations can lead to rotational transitions there can be ambiguity. In this chlorobutyne example, when measuring the spectrum of an eigenstate with $J = 4$, we expect that the frequency for a $\Delta J = +1$ transition from the *trans* contribution will lie in the same frequency range as a $\Delta J = -1$ transition of the *gauche* conformer. Our triple-resonance technique allows us to determine the 'sign' of the observed transition frequencies. Additionally, the method provides a direct measure of the square of the transition moment independent of which eigenstate is probed.

Examples of the $J = 4 \rightarrow J = 3$ rotational spectra for four different single eigenstates are shown in figure 21. The rotational spectra of these eigenstates are much richer than the single transition frequency spectra associated with low energy rotational motion. The presence of IVR and isomerization leads to spectra that cover a wide range of frequencies ($\sim$10 GHz). A composite spectrum, obtained by simply combining the four spectra of figure 21, is shown in figure 22. In this figure we also show the composite spectrum of the $J = 4 \rightarrow J = 5$ transitions. The $\Delta J = +1$ and $\Delta J = -1$ composite spectra (figure 22) originate from the same set of eigenstates. Note that the two spectra overlap in frequency. The observation of rotational transitions from a single eigenstate at frequencies characteristic of both the *trans* and *gauche* conformers clearly demonstrates that these eigenstates contain contributions from zeroth-order states associated with both conformers. As indicated by the calculation presented in figure 14, the isomerization rate can be determined by analysing the overall line shape profile of the single eigenstate spectra. In both

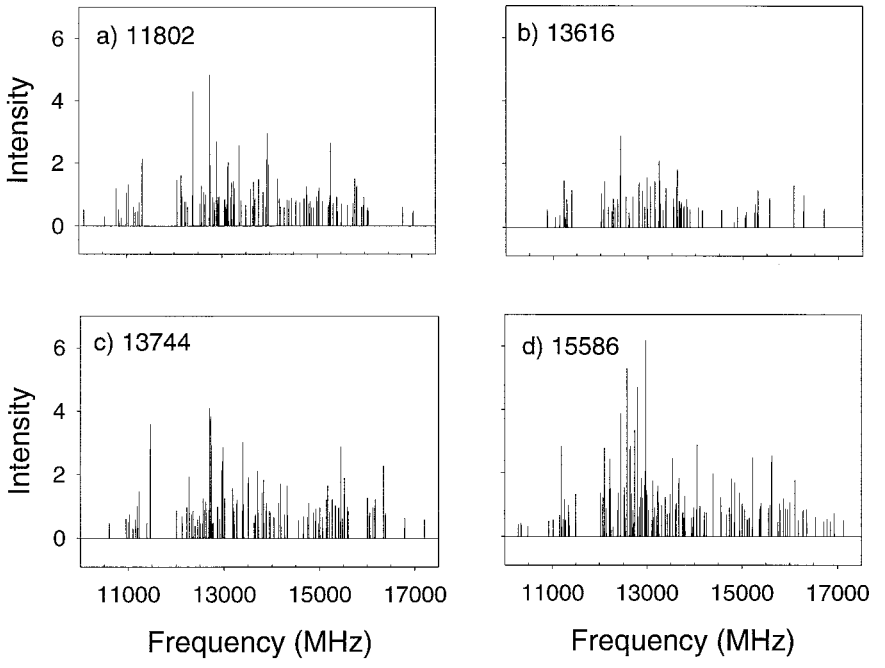

Figure 21. Four examples of the rotational spectrum of a single quantum state of chlorobutyne are shown. The eigenstates all have rotational quantum number $J = 4$ and are prepared through double-resonance spectroscopy (the 11 802 MHz transition in figure 20 yields the spectrum shown in (*a*)). Only transitions to lower energy quantum states (i.e. $J = 4 \rightarrow J = 3$) are shown. By comparing the observed frequencies to those calculated in figure 12, it is clear that each single quantum state contains contributions from both *trans* and *gauche* zeroth-order states.

transitions of figure 22 we show the predicted line shape profile for an isomerization rate of $1.2 \times 10^{10}\ s^{-1}$ ($\tau_{isom} = 84$ ps).

The effects of isomerization on the rotational spectrum are further illustrated in figure 23. In this figure we show the rotational spectrum that would be expected in the case of very slow isomerization. To calculate this spectrum we predict the rotational transition frequency for each torsional state of the 1D potential. These frequencies are calculated by determining the average rotational constants for the torsional state using the *ab initio* values of the rotational constants at each different torsional angle [67, 68, 90, 96]. This model assumes that the main vibrational dependence of the rotational constant is given by the torsional contribution. The method of calculating rotational constants by averaging over the large amplitude wavefunction has been used successfully to describe the rotational spectra of molecules with an isomerization coordinate [90, 96] and weakly bound complexes [67, 68]. The solid line in figure 23 shows the overall line shape profile in the presence of isomerization (this profile is the same as the one in figure 22). The changes in the rotational spectrum indicate the approach to coalescence in the rotational spectrum.

One interesting result of this study is the fact that the isomerization rate from the single eigenstate rotational spectroscopy ($1.2 \times 10^{10}\ s^{-1}$) is significantly faster than the upper limit rate determined from the survival probability of the acetylenic C–H stretch ($3.3 \times 10^{8}\ s^{-1}$). However, the single eigenstate result is still significantly slower

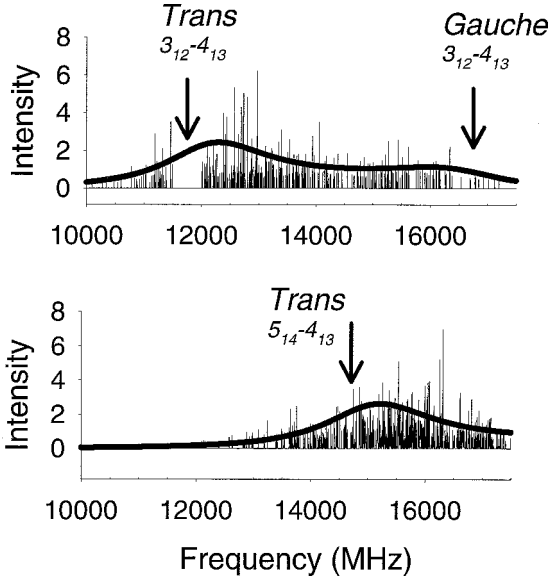

Figure 22. The *trans–gauche* isomerization rate for chlorobutyne can be determined by analysing the overall line shape profile of the single eigenstate rotation spectra (see figure 14). For the analysis, the spectra for all four states of figure 21 are combined to give a composite spectrum. The overall line shape profile for both the $J = 4 \rightarrow J = 3$ and the $J = 4 \rightarrow J = 5$ is shown by the solid line for an isomerization lifetime of 84 ps. The arrows in the figure indicate the expected rotational frequencies for the ground state *trans* and *gauche* conformers.

than the RRKM value ($1 \times 10^{13} s^{-1}$). The comparison of the two measurements shows that the isomerization process is strongly mode-specific in chlorobutyne. In other words, the observed isomerization rate depends critically on how the vibrational energy is initially distributed within the molecule (e.g. localized in a single bond (infrared bright-state measurement) or redistributed throughout the molecule (single eigenstate measurements)). Previous theoretical work has suggested that isomerization reactions, as a class, will violate RRKM predictions [104, 105]. Our work on chlorobutyne [10, 103] and 2-fluoroethanol [9] supports this result.

4.2. *Generalizations of the method*

In this review, we have focused on the description of the rotational spectroscopy of quantum states in energy regions where state-mixing is extensive. When the molecule is in an energy region where intramolecular dynamics occur, the description of the spectroscopy must include the effects of nuclear motion. These effects are not required for the low-energy quantum states investigated in the vast majority of spectroscopy studies and so are often omitted from molecular spectroscopy treatments [1, 2, 14, 15]. As illustrated in the previous section, the fact that motion, such as isomerization, has such drastic effects on spectral line shape means that frequency-domain techniques can be used to obtain quantitative kinetics data.

Although we have presented the rotational spectroscopy problem, the general ideas are valid for any form of spectroscopy. In fact, many of the basic issues of IVR exchange narrowing have been studied for vibrational spectroscopy in the context of

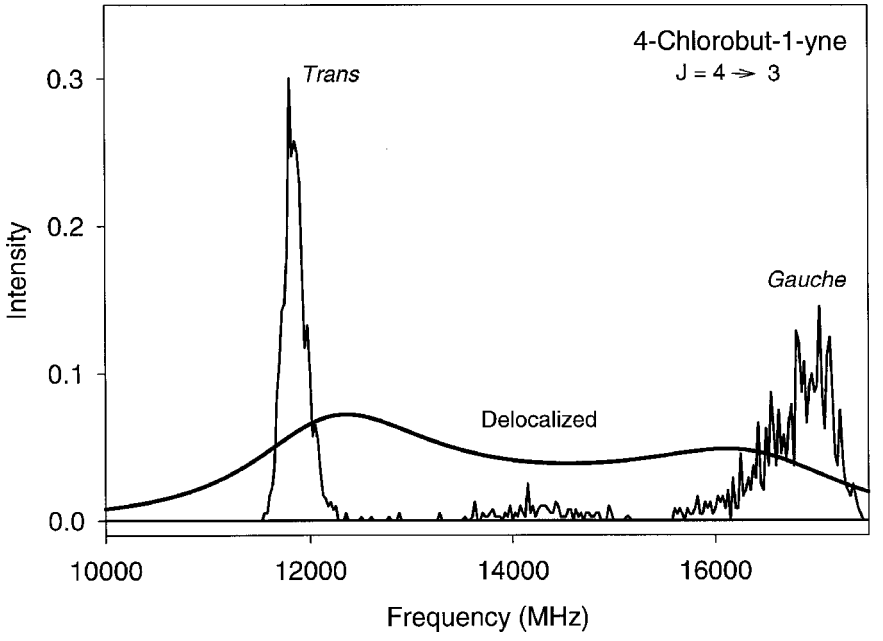

Figure 23. This figure further illustrates how the isomerization dynamics have modified the overall line shape profile of the single quantum state rotational spectra. The smooth solid curve shows the overall line shape observed in the experiment (see figure 22) and corresponds to an isomerization lifetime of 84 ps. Underneath this curve we show the zeroth-order distribution of rotational frequencies expected at 3330 cm^{-1}. This distribution is calculated by using a direct state count algorithm to identify all quantum states near 3330 cm^{-1} and then estimating their rotational frequency based on the torsional wavefunction using the calculation of figure 12. The observed line shape profile shows the 'frequency pulling' effects of the coalescence phenomenon (figure 14).

infrared multiphoton excitation [49, 50, 51, 52]. In terms of isomerization reactions, other forms of spectroscopy, such as vibrational spectroscopy of structurally mixed states, offer significant advantages. For conformational isomerization reactions, the vibrational frequencies of the molecule depend on the molecular structure. The frequency differences for some normal-mode vibrations can differ by 10 cm^{-1} or more for the different geometries [35, 36, 37]. This magnitude of transition frequency difference would be useful for kinetics measurements in the case where there is exceptionally fast isomerization.

For higher energy isomerization reactions, such as the ones indicated in figure 24, single eigenstate spectroscopy can provide new insight into the kinetics. This approach holds the possibility, for example, of measuring the vibrational spectrum of the transition state geometry. For reactions such as the propene/cyclopropane reaction, the characteristic vibrational frequencies of the stable isomers are quite distinct. The emergence of transition state vibrational features should be readily apparent. These spectra would be expected to reveal new information about the microcanonical rate constants and the reaction pathway for these fundamental reactions. In this way, *frequency-domain* techniques can be used to obtain information on the structure and dynamics of the transition state.

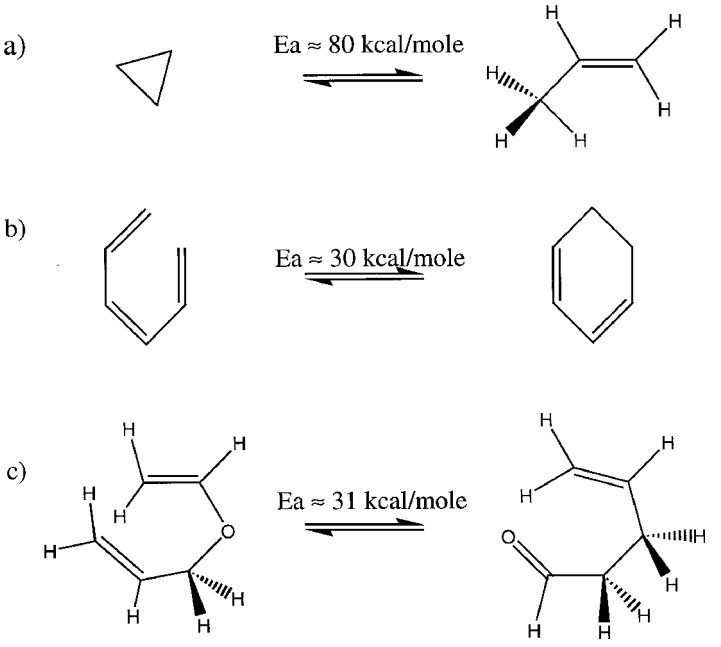

Figure 24. This figure shows some typical high-barrier isomerization reactions of general chemical interest. In all cases, the isomerization reaction proceeds without unimolecular dissociation. As a result, the molecular eigenstates will be discrete. Each molecular eigenstate will contain contributions from the zeroth-order reactant, product and transition state structures. For example, structurally mixed quantum states of the first reaction are expected to simultaneously show properties of the closed cyclopropane structure and the open propene structure. Frequency-domain spectroscopy of these structurally mixed states can be used to study the kinetics of this class of reactions through the spectroscopic effects described in this review.

Measurements of the spectroscopy of structurally mixed states of high-barrier reactions will challenge our chemical ideas about molecular structure. For example, the simple Claissen rearrangement of figure 24 (*c*) remains bound at all times. Therefore, the eigenstates at high energy must, in a sense, be simultaneously aldehyde-like and ether-like. In this reaction, obtaining the electronic spectrum of the mixed-states would be an interesting measurement since it should clearly distinguish the aldehyde and the ether contributions to the eigenstate.

Finally we suggest that the spectroscopy of structurally mixed quantum states opens up new avenues for performing selective chemistry with lasers. The traditional approach to laser chemistry has been to pursue bond-localized excitation to achieve bond-selective reactivity [109]. In principle, this approach is valid as demonstrated by the work of Crim and co-workers using small polyatomic molecules [110, 111]. However, for large molecules the time scale for energy localization in a bond is typically too short to permit a reactive encounter with the energy-localized molecule.

As an alternative, one can direct the outcome of a wide range of chemical reactions by controlling the geometry of the reactant [112, 113]. Therefore, the control of the molecular structure can be converted into reaction product control. In this approach, the properties of structurally mixed quantum states are potentially useful. As discussed in the previous section, it is possible to 'make' any structure

of the molecule that is expressed in the wavefunction using light pulses that can distinguish the different geometries. The basic idea that the variation of absorption frequencies can be used to distinguish isomers has been used to reversibly drive several isomerization reactions using infrared multiphoton excitation [114, 115, 116, 117, 118]. The advances in laser technology since these experiments now permits much more precise control over the excitation sequence. This improved control should make it possible to manipulate molecular structure and, therefore, chemical reactivity, using simple laser pulse sequences.

5. Conclusions

The general trend in molecular spectroscopy is the development of techniques to study larger molecules at higher energy [21, 23, 24]. In this pursuit, important new features of intramolecular dynamics affect the appearance of the spectrum. For example, the IVR process leads to fragmentation of the transition intensity across several molecular eigenstates. The interpretation of this effect, as described by figure 1, is now a well-known problem in molecular spectroscopy [24]. In this review, we have described a new type of methodology that considers the spectroscopy between molecular eigenstates in an energy region where IVR occurs. Here new features show up in the description of the spectroscopy between the highly mixed states that result from IVR. During the rotational motion of the molecule it is now necessary to consider the nuclear motion that accompanies vibrational energy flow and isomerization. These effects are not encountered in the low energy regime where regular, near-harmonic vibration occurs on a time scale that is rapid compared to rotation. In this regime, the effects of nuclear vibrational motion during rotation can be included through the vibrational dependence of the rotational constant. In the regime we have considered, the vibrational energy flow leads to dramatic departures from traditional rotational spectroscopy. These new effects in the single eigenstate rotational spectra are described using the motional narrowing theories from NMR spectroscopy.

Rotational spectroscopy in the IVR regime is especially useful for measuring the kinetics of unimolecular isomerization reactions. Because these reactions do not lead to dissociation, the molecular quantum states remain discrete. Within the zeroth-order model that separates small amplitude normal-mode vibrations from nuclear motion along the isomerization coordinate, as depicted in figure 4, isomerization leads to eigenstates that are 'structurally mixed'. Each individual quantum state contains contributions from the reactant, product and transition state structures. Through the structural-dependence of the rotational frequency, it is possible to probe these separate contributions to the quantum state. In this way it is possible to measure the rotational spectrum of reactive intermediates and transition states using frequency-domain techniques. In the near future, we expect that this form of spectroscopy will be extended to study reactions at higher energy. Different types of spectroscopy measurements on highly mixed states, such as performing vibrational or electronic spectroscopy, are also expected to see development in this direction. Finally, because the spectroscopy in the presence of IVR shares many features with NMR spectroscopy, the development of time-domain techniques [119] should provide improved methods for extracting the intramolecular dynamics and, possibly, for manipulating nuclear geometry and motion.

Acknowledgments

This work has been supported by the Career Program of the National Science Foundation (CHE-9624850), the Camille and Henry Dreyfus Foundation and the Jeffress Foundation. We would like to thank Dr Chung Yi Lee, Grant Hudspeth, David Green and Rebecca Holmberg for their contributions to the development of single eigenstate rotational spectroscopy. We would also like to thank Kevin Lehmann and Jerry Fraser for many helpful discussions of the spectroscopy of highly mixed states.

References

[1] Townes, C. H., and Schawlow, A. L., 1975, *Microwave Spectroscopy* (New York: Dover Publications).
[2] Gordy, W., and Cook, R. L., 1984, *Microwave Molecular Spectra*, 3rd edn (New York: Wiley).
[3] Slichter, C. P., 1996, *Principles of Magnetic Resonance*, 3rd edn (New York: Springer).
[4] Abragam, A., 1996 *Principles of Nuclear Magnetism* (Oxford: Clarendon Press).
[5] Robinson, P. J., and Holbrook, K. A., 1972, *Unimolecular Reactions* (New York: Wiley-Interscience).
[6] Baer, T., and Hase, W. L., 1996, *Unimolecular Reaction Dynamics: Theory and Experiments* (New York: Oxford University Press).
[7] Heller, E. J., and Gelbart, W. M., 1980. *J. chem. Phys.*, **73,** 626.
[8] Keske, J. C., and Pate, B. H., 2000, *Chem. Phys. Lett.* (submitted).
[9] Lee, C. Y., and Pate, B. H., 1997, *J. chem. Phys.*, **107,** 10430.
[10] McWhorter, D. A., Hudspeth, E., and Pate, B. H., 1999, *J. chem. Phys.*, **110,** 2000.
[11] Bixon, M., and Jortner, J., 1968, *J. chem. Phys.*, **48,** 715.
[12] Stannard, P. R., and Gelbart, W. M., 1981, *J. Phys. Chem.*, **85,** 3592.
[13] Freed, K. F., and Nitzan, A., 1980, *J. chem. Phys.*, **73,** 4765.
[14] Herzberg, G., 1945, *Molecular Spectra and Molecular Structure II. Infrared and Raman Spectra of Polyatomic Molecules* (New York: Van Nostrand Reinhold).
[15] Papousek, D., and Aliev, M. R., 1982, *Molecular Vibrational-Rotational Spectra* (New York: Elsevier).
[16] Lawrance, W. D., and Knight, A. E. W., 1988, *J. Phys. Chem.*, **92,** 5900.
[17] de Souza, A. M., Kaur, D., and Perry, D. S., 1988, *J. chem. Phys.*, **88,** 4569.
[18] McIlroy, A., and Nesbitt, D. J., 1989, *J. chem. Phys.*, **92,** 2229.
[19] Pate, B. H., Lehmann, K. K., and Scoles, G., 1991, *J. chem. Phys.*, **95,** 3891.
[20] Miller, C. C., Philips, L. A., Andrews, A. M., Fraser, G. T., Pate, B. H., and Suenram, R. D., 1994, *J. chem. Phys.*, **100,** 831.
[21] Lehmann, K. K., Scoles, G., and Pate, B. H., 1994, *Ann. Rev. Phys. Chem.*, **45,** 241.
[22] Fraser, G. T., Pate, B. H., Bethardy, G. A., and Perry, D. S., 1993, *Chem. Phys.*, **175,** 223
[23] Keske, J. C., and Pate, B. H., 2000, *Ann. Rev. Phys. Chem.*, **51** (in the press).
[24] Nesbitt, D. J., and Field, R. W., 1996, *J. Phys. Chem.*, **100,** 12735.
[25] Jiang, X. P., and Brumer, P., 1991, *J. chem. Phys.*, **94,** 5833.
[26] Wynne, K., and Hochstrasser, R. M., 1995, *Chem. Phys.*, **193,** 211.
[27] Khundkar, L. R., and Zewail, A. H., 1990, *Ann. Rev. Phys. Chem.*, **41,** 15.
[28] Heller, E. J., 1980, *J. chem. Phys.*, **72,** 1337.
[29] Green, D., Hammond, S., Keske, J., and Pate, B. H., 1999, *J. chem. Phys.*, **110,** 1979.
[30] Bigwood, R., and Gruebele, M., 1995, *Chem. Phys. Lett.*, **235,** 604.
[31] Gruebele, M., 1996, *J. phys. Chem.*, **100,** 12183.
[32] Gruebele, M., and Bigwood, R., 1998, *Int. Rev. Phys. Chem.*, **17,** 91.
[33] Carrington, T., Hubbard, L. M., Schaefer, H. F., and Miller, W. H., 1984. *J. chem. Phys.*, **80,** 4347.
[34] Hudspeth, E., McWhorter, D. A., and Pate, B. H., 1997, *J. chem. Phys.*, **107,** 8189.
[35] Kalasinsky, V. F., and Pechsiri, S., 1980, *J. Raman. Spectrosc.*, **9,** 120
[36] Durig, J. R., Yu, Z., and Gurgis, G. A., 1999, *J. Molec. Struct.*, **509,** 115.
[37] Durig, J. R., Nashed, Y. E., Jin, Y. P., and Gurgis, G. A., 1998, *J. Molec. Struct.*, **449,** 1.

[38] Stewart, G. M., and McDonald, J. D., 1981, *J. chem. Phys.*, **75,** 5949.
[39] Kim, H. L., Kulp, T. J., and McDonald, J. D., 1987, *J. chem. Phys.*, **87,** 4376.
[40] Anderson, D. T., Schuder, M., and Nesbitt, D. J., 1998, *Chem. Phys.*, **239,** 253.
[41] Fraser, G., 1991, *Int. Rev. Phys. Chem.*, **10,** 189.
[42] Liu, K. Cruzan, J. D., and Saykally, R. J., 1996, *Science*, **271,** 929.
[43] Kay, K. G., 1981, *J. chem. Phys.*, **75,** 1690.
[44] Stone, J., Thiele, E., and Goodman, M. F., 1981, *J. chem. Phys.*, **75,** 1712.
[45] Mukamel, S., 1979, *J. chem. Phys.*, **70,** 5834.
[46] Schek, I., and Jortner, J., 1978, *J. chem. Phys.*, **70,** 3016.
[47] Stuchebrukhov, A., Ionov, S., and Letokhov, V., 1989, *J. Phys. Chem.*, **93,** 5357.
[48] Letokhov, V. S., 1989, *Laser Spectroscopy of Highly Vibrationally Excited Molecules* (New York: Adam Hilger).
[49] Bagratashvili, V. N., Burimov, V. N., Ionov, S. I., Sviridov, A. P., Stuchebrukhov, A. A., and Turovetz, I. M., 1987, *Chem. Phys. Lett.*, **137,** 45.
[50] Bagratashvili, V. N., Ionov, S., Stuchebrukhov, A. A., Letokhov, V. S., Lokhman, V. N., and Makarov, A. A., 1988, *Chem. Phys. Lett.*, **146,** 599.
[51] Malinovsky, A. L., Ryabov, E. A., and Letokhov, V. S., 1989, *Chem. Phys.*, **139,** 229.
[52] Malinovsky, A. L., Petrova, I. Y., Ryabov, E. A., Makarov, A. A., and Letokhov, V. S., 1998, *J. Phys. Chem.* A, **102,** 9353.
[53] Fleming, P. R., Li, M., and Rizzo, T. R., 1991, *J. chem. Phys.*, **94,** 2425.
[54] Fleming, P. R., and Rizzo, T. R., 1991, *J. chem. Phys.*, **95,** 1461.
[55] Boyarkin, O. V., Rizzo, T. R., and Perry, D. S., 1997, *J. chem. Phys.*, **107,** 8409.
[56] Boyarkin, O. V., Rizzo, T. R., and Perry, D. S., 1999, *J. chem. Phys.*, **110,** 11346.
[57] Boyarkin, O. V., Rizzo, T. R., and Perry, D. S., 1999, *J. chem. Phys.*, **110,** 11359.
[58] Romanini, D., and Lehmann, K. K., 1993, *J. chem. Phys.*, **99,** 6287.
[59] Lehmann, K. K., and Smith, A. M., 1990, *J. chem. Phys.*, **93,** 6140.
[60] Makarov, A. A., 1987, *Opt. Spectrosc.* (USSR), **62,** 697.
[61] Pate, B. H., 1998, *J. chem. Phys.*, **109,** 4396.
[62] Pate, B. H., 1999, *J. chem. Phys.*, **110,** 1990.
[63] Anderson, P. W., and Weiss, P. R., 1953, *Rev. Mod. Phys.*, **25,** 269.
[64] Anderson, P. W., 1954, *J. phys. Soc. Jpn.*, **9,** 316.
[65] Kubo, R., and Tomita, K., 1954, *J. Phys. Soc. Jpn.*, **9,** 888.
[66] Van Vleck, J. H., 1948, *Phys. Rev.*, **74,** 1168.
[67] Sabo, D., Bacic, Z., Graf, S., and Leutwyler, S., 1999, *J. chem. Phys.*, **111,** 10727.
[68] Sabo, D., Bacic, Z., Graf, S., and Leutwyler, S., 1999, *J. chem. Phys.*, **110,** 5745.
[69] Gambogi, J. E., Kerstel, E. R. Th., Yang, X., Lehmann, K. K., and Scoles, G., 1996, *J. Molec. Spectrosc.*, **175,** 198.
[70] Gambogi, J. E., Kerstel, E. R. T., Lehmann, K. K., and Scoles, G., 1994, *J. chem. Phys.*, **100,** 2612.
[71] Perry, D. S., 1993, *J. chem. Phys.*, **98,** 6665.
[72] Go, J., and Perry, D. S., 1995, *J. chem. Phys.*, **103,** 5194.
[73] Wilkinson, M., 1988, *J. Phys.* A, **21,** 1173.
[74] Chirikov, B. V., 1979, *Phys. Rep.*, **52,** 265.
[75] Hudspeth, E., McWhorter, D. A., and Pate, B. H., 1998, *J. chem. Phys.*, **109,** 4316.
[76] Green, D., Holmberg, R., Lee, C. Y., McWhorter, D. A., and Pate, B. H., 1998, *J. chem. Phys.*, **109,** 4407.
[77] Li, H., Ezra, G. S., and Philips, L. A., 1992, *J. chem. Phys.*, **97,** 5956.
[78] Kakar, R., and Quade, C. R., 1998, *J. chem. Phys.*, **72,** 4300.
[79] Liu, M., and Quade, C. R., 1991, *J. Molec. Spectrosc.*, **146,** 238.
[80] Hirota, E., 1970, *J. Molec. Spectrosc.*, **35,** 9.
[81] Kondo, S., Hirota, E., and Morino, Y., 1968, *J. Molec. Spectrosc.*, **28,** 471.
[82] Meakin, P., Harris, D. O., and Hirota, E., 1969, *J. chem. Phys.*, **51,** 3775.
[83] Stiefvater, O. L., and Wilson, E. B., 1969, *J. chem. Phys.*, **50,** 5385.
[84] Wodarczyk, F. J., and Wilson, E. B., 1972, *J. chem. Phys.*, **56,** 166.
[85] Fraser, G. T., Suenram, R. D., and Lugez, C. L., 2000, *J. Phys. Chem.* (in the press).
[86] Durig, J. R., Yu, Z. Gurgis, G. A., Little, T. S., Zhen, M., and Lee, M. J., 1998, *J. Phys. Chem.* A, **102,** 10460.

[87] DURIG, D. T., GUIRGUS, G. A., BELL, S., and BREWER, W. E., 1997, *J. Phys. Chem.* A, **101,** 9240.
[88] LEWIS, J. D., MALLOY, T. B., CHAO, T. H., and LAANE, J., 1972, *J. Molec. Struct.*, **12,** 427
[89] MCWHORTER, D. A., and PATE, B. H., 1998, *J. Phys. Chem.* A, **102,** 8786.
[90] MCWHORTER, D. A., and PATE, B. H., 1998, *J. Phys. Chem.* A, **102,** 8795.
[91] ELIASON, M. A., and HIRSCHFELDER, J. O., 1959, *J. chem. Phys.*, **30,** 1426.
[92] HOFACTOR, L., 1963, *Z. Naturforsch.*, **18A,** 607.
[93] MILES, F. H., 1969, *J. chem. Phys.*, **51,** 798.
[94] MARCUS, R. A., 1996, *J. chem. Phys.*, **45,** 4493.
[95] QUACK, M., and TROE, J., 1974, *Ber. Bunsenges. Phys. Chem.*, **78,** 240.
[96] MEYER, R., and WILSON, E. B., 1970, *J. chem. Phys.*, **53,** 3969.
[97] GÜNTHER, H., 1995, *NMR Spectroscopy: Basic Principles, Concepts, and Applications in Chemistry*, 2nd edn (New York: Wiley).
[98] MCWHORTER, D. A., 1998, PhD thesis, University of Virginia, USA.
[99] GUTOWSKY, H. S., MCCALL, D. W., and SLICHTER, C. P., 1953, *J. chem. Phys.*, **21,** 279.
[100] GUTOWSKY, H. S., and HOLM, C., 1956, *J. chem. Phys.*, **25,** 1228.
[101] MCCONNELL, H. M., 1958, *J. chem. Phys.*, **28,** 430.
[102] STEINFELD, J. I., FRANCISCO, J. S., and HASE, W. L., 1989, *Chemical Kinetics and Dynamics* (London: Prentice-Hall).
[103] KESKE, J. C., and PATE, B. H., 2000, *J. chem. Phys.* (submitted)
[104] LEITNER, D. M., and WOLYNES, P. G., 1997, *Chem. Phys. Lett.*, **280,** 411.
[105] BORCHARDT, D. B., and BAUER, S. H., 1986, *J. chem. Phys.*, **85,** 4980.
[106] FRISCH, M. J., TRUCKS, G. W., SCHLEGEL, H. B., GILL, P. M. W., JOHNSON, B. J., ROBB, M. A., CHEESEMAN, J. R., KEITH, T. A., PETERSSON, G. A., MONTGOMERY, J. A., RAGHAVACHARI, K, AL-LAHAM, L. A., ZAKRZEWSKI, V. G., ORTIZ, J. V., FORESMAN, J. B., CIOSLOWSKI, J., STEFANOW, B. B., NANAYAKLARA, A., CHALLACOMBE, M., PENG, C. Y., AYALA, P. Y., CHEN, W., WONG, M. W., ANDERS, J. L., REPLOGLE, E. S., GOMPERTS, R., MARTIN, R. L., FOX, D. J., BINKLEY, J. S., DEFREES, D. J., BAKER, J., STEWART, J. P., HEAD-GORDON, M., GONZALEZ, C., and POPLE, J. A., 1995, GAUSSIAN 98, Version 5.1 (Pittsburgh PA: Gaussian, Inc.).
[107] SUHM, M. A., FARRELL JR, J. T., ASHWORTH, S. H., and NESBITT, D. J., 1993, *J. chem. Phys.*, **98,** 5985.
[108] CUPP, S., LEE, C. Y., MCWHORTER, D., and PATE, B. H., 1998, *J. chem. Phys.*, **109,** 4302.
[109] ZEWAIL, A. H., 1980, *Phys. Today*, 513.
[110] CRIM, F. F., 1999, *Acc. Chem. Res.*, **32,** 877.
[111] BERGHOUT, H. L., CRIM, F. F., ZYRIANOV, M., and REISLER, H., 2000, *J. chem. Phys.* (in the press).
[112] WAGNER, P. J., 1983, *Acc. Chem. Res.*, **16,** 461.
[113] SEEMAN, J. I., 1983, *Chem. Rev.*, **83,** 83.
[114] DANEN, W. C., KOSTER, D. F., and ZITTER, R. N., 1979, *J. Am. Chem. Soc.*, **79,** 1501.
[115] FARNETH, W. E., THOMSEN, M. W., SCHULTZ, N. L., and DAVIES, M. A., 1981, *J. Am. Chem. Soc.*, **103,** 4001.
[116] TENG, P. P., WEITZ, E., and LEWIS, F. D., 1999, *J. Am. Chem. Soc.*, **104,** 5518.
[117] BUECHELE, J. L., WEITZ, E., and LEWIS, F. D., 1982, *J. chem. Phys.*, **77,** 3500.
[118] LEWIS, F. D., TENG, P. P., and WEITZ, E., 1983, *J. Phys. Chem.*, **87,** 1666.
[119] MAKAROV, A. A., 1992, *Chem. Phys. Lett.*, **190,** 236.